Recent Advancements for Tropical Cyclone Data Assimilation

Hui Christophersen[1], Jason Sippel[2], Altug Aksoy[3], and Nancy L. Baker[1]

[1]Naval Research Laboratory, Monterey, California

[2]NOAA/Atlantic Oceanographic and Meteorological Laboratory/Hurricane Research Division, Miami, Florida

[3]Cooperative Institute for Marine and Atmospheric Studies, University of Miami, and NOAA/Atlantic Oceanographic and Meteorological Laboratory/Hurricane Research Division, Miami, Florida

Abstract

In this review, data assimilation (DA) techniques used for tropical cyclones (TCs) are briefly overviewed. The strength and weakness of variational methods, ensemble methods, hybrid methods and particle filter methods are also discussed. Several global numerical weather prediction (NWP) models and their corresponding DA systems frequently used for TC forecasting and verification are described first. The DA research and development (R&D) efforts in the operational regional model from the National Centers for Environmental Prediction (NCEP)'s Hurricane Weather Research and Forecasting (HWRF) are then discussed in greater detail. Focused remarks on TC observations from reconnaissance, ground-based radar, enhanced satellite-derived atmospheric motion vectors (AMVs) and all-sky satellite radiances and their impacts on TC analyses and forecasts are addressed. Recent TC DA advancements and challenges on better use of observations and more advanced DA methods for TC application are also briefly reviewed.

Keywords: tropical cyclone, data assimilation, numerical weather prediction

For publication in

Annals of the New York Academy of Sciences

1. Brief Review of Contemporary Data Assimilation Techniques

Data assimilation (DA) is the process of combining a recent model background state and observations into an analysis that represents the best estimate of the current state of the atmosphere. This is then typically used as the initial conditions of a new model forecast or to investigate the physical structure of the atmosphere within the model domain. A number of approaches to DA have been proposed in recent decades, and it should be noted that in the limit of a linear model, linear observations of the model, and uncorrelated Gaussian errors, all of these approaches can be reduced to the same basic Bayesian principles. However, adding nonlinearity and complexity in any of these components introduces departures from the optimal Bayesian solution. In the following, a brief overview of the various approaches that were introduced over the past several decades is provided as they apply to TC DA. While TC DA uses these fundamental approaches, there are various challenges for TC applications (e.g., how to tailor to TC's multi-scales, spatiotemporal observational challenges, etc). We provide a brief overview in section 5 to address the advancements and challenges in TC DA applications. For further detailed reading about DA approaches, the following review articles are recommended as good starting points: Ref. 1 for variational methods, Ref. 2 for ensemble methods, and Ref. 3 for particle filter methods.

1.1 Variational methods

In variational DA, the goal is to obtain an optimal analysis solution by defining and minimizing a cost function. As early as in the 1980s, the formulation of this problem was available,[4] although further modifications were made to allow for time evolution and model error to arrive at the following generalized definition of the cost function J,

$$
\begin{aligned}
J(\mathbf{x}_0) = & \frac{1}{2}\left(\mathbf{x}_0 - \mathbf{x}_0^b\right)^T \mathbf{B}_0^{-1}\left(\mathbf{x}_0 - \mathbf{x}_0^b\right) \\
& + \frac{1}{2}\sum_{t=0}^{T}(\mathbf{y}_t^o - H\mathbf{x}_t)^T \mathbf{R}_t^{-1}(\mathbf{y}_t^o - H\mathbf{x}_t) \\
& + \frac{1}{2}\sum_{t=1}^{T}(\mathbf{x}_{t+1} - M\mathbf{x}_t)^T \mathbf{Q}_t^{-1}(\mathbf{x}_{t+1} - M\mathbf{x}_t),
\end{aligned}
$$

where $\mathbf{x}$, $\mathbf{y}^o$, and t represent the model state, observed state, and time, respectively. Furthermore, $\mathbf{B}$, $\mathbf{R}$ and $\mathbf{Q}_t$ denote the background-error covariance matrix, observation-error covariance matrix, and model-error covariance matrix, respectively. H represents the nonlinear observation forward operator, and M is the nonlinear model.

In the original, three-dimensional variational (3DVar) formulation,[5] only the first two terms are defined, and without the time dimension (i.e., all terms are valid at t=0). The first term is known as the "background term" and represents the departure of the analysis state ($\mathbf{x}$) from the background state ($\mathbf{x}^b$) weighted by the background-error covariance matrix ($\mathbf{B}$). The second term is called the "observation term" and measures the deviation of the analysis state ($\mathbf{x}$) from the observed state ($\mathbf{y}^o$) weighted by the observation-error covariance matrix ($\mathbf{R}$). The observation forward operator (H) is needed for the transformation from model space to observation space. The analysis state $\mathbf{x}^a$ is generally obtained by setting the derivative of the cost function to zero, i.e., $\nabla_x J(\mathbf{x}^a) = 0$, and applying iterative techniques.

Further generalization that allows for the second (observation) term of the cost function to be evaluated at multiple times was later developed and became known as the four-dimensional variational (4DVar) formulation.[6] The main advantage of the 4DVar against the 3DVar is its ability to evaluate the observation term over multiple (shorter) time steps that more realistically represent the actual time of the observations and also results in smaller observed-analysis differences and a more-linearized response within the forward operator. However, the intermediate state at each of these time steps is obtained by the model integration $\mathbf{x}_t = M\mathbf{x}_{t-1}$, thus forcing these steps to be constrained purely by the model dynamics. This perfect-model assumption of the original 4DVar was later termed as the strong-constraint formulation.

To relax the strong constraint that requires a solution to fit the model trajectory at all times, the third term of the cost function was proposed,[7] which defines the model-error covariance matrix ($\mathbf{Q}_t$) as random forcing that allows for $\mathbf{x}_t$ to deviate from the model trajectory, thus $\mathbf{x}_t - M\mathbf{x}_{t-1} \neq 0$. This most generalized variational formulation is commonly referred to as the weak-constraint 4DVar.

The cost function defined above involves full model fields. This general definition requires nonlinear operators *M* and *H* and results in a non-quadratic form of the cost function that is difficult to minimize numerically. Therefore, further algorithmic simplification can be achieved if *M* and *H* are linearized so that the cost function becomes quadratic. If one thus defines the state and model error terms as perturbations around the background state ($\mathbf{x}^b$) so that $\boldsymbol{x}_t = \boldsymbol{x}_t^b + \delta\boldsymbol{x}_t$ and $\boldsymbol{\eta}_t = \delta\boldsymbol{\eta}_t$ (i.e. only random model error), and further defines the linearized model as $\mathbf{M}_{t-1,t} = \partial\mathbf{x}_t/\partial\mathbf{x}_{t-1}$, one can obtain the following linearized approximation for the state increment:

$$\delta\mathbf{x}_t \approx M_{0,t}\delta\boldsymbol{x}_0 + \sum_{\tau=1}^{T}\mathbf{M}_{\tau,t}\delta\boldsymbol{\eta}_\tau.$$

Similarly, the forward operator can be approximated as follows:

$$H\mathbf{x}_t \approx H\mathbf{x}_t^b + \mathbf{H}_t\delta\mathbf{x}_t,$$

where $\mathbf{H}_t = \partial\mathbf{y}_t/\partial\mathbf{x}_t$. With these linear approximations, one obtains the following incremental form of the weak-constraint cost function

$$\begin{aligned} J(\delta\mathbf{x}_0, \delta\boldsymbol{\eta}) = {} & \frac{1}{2}(\delta\mathbf{x}_0)^T\mathbf{B}_0^{-1}(\delta\mathbf{x}_0) \\ & + \frac{1}{2}\sum_{t=0}^{T}\left(\mathbf{y}_t^o - H\mathbf{x}_t^b - \mathbf{H}_t\delta\mathbf{x}_t\right)\mathbf{R}_t^{-1}\left(\mathbf{y}_t^o - H\mathbf{x}_t^b - \mathbf{H}_t\delta\mathbf{x}_t\right)^T \\ & + \frac{1}{2}\sum_{t=1}^{T}(\delta\boldsymbol{\eta}_t)^T\mathbf{Q}_t^{-1}(\delta\boldsymbol{\eta}_t), \end{aligned}$$

which is minimized over an inner loop. It should also be noted that this is the generalization of the strong-constraint incremental formulation first proposed by Courtier et al.[8]

A further transformation should finally be mentioned, which will become important in discussing the hybrid methods. Even though the incremental formulation described above circumvents the complexities

of minimizing a non-quadratic cost function, it still involves explicit definitions of matrices $\mathbf{B}_0$, $\mathbf{R}_t$, and $\mathbf{Q}_t$, which are typically very large in dimension. To avoid this issue, a change of variables is proposed that simplifies the background, observation error and model error terms as follows:

$$\delta\mathbf{x} = \mathbf{U}\delta\boldsymbol{\chi},$$
$$\delta\boldsymbol{\eta}_t = \mathbf{V}_t\delta\boldsymbol{\gamma}_t.$$

The new variables $\delta\boldsymbol{\chi}$ and $\delta\boldsymbol{\gamma}_t$ are known as "control variables" and the matrices $\mathbf{U}$ and $\mathbf{V}_t$ are control variable transforms (CVTs). The idea is to choose control variables in such a way that their error covariances are $\mathbf{I}$; i.e., $\mathbf{U}^T\mathbf{B}_0^{-1}\mathbf{U} = \mathbf{I}$ and $\mathbf{V}_t^T\mathbf{Q}_t^{-1}\mathbf{V}_t = \mathbf{I}$, which leads to the much simpler formulation of the cost function as follows:

$$J(\delta\boldsymbol{\chi}, \delta\boldsymbol{\gamma}_t) = \frac{1}{2}(\boldsymbol{\chi})^T(\boldsymbol{\chi}) + \frac{1}{2}\sum_{t=0}^{T}\left(\mathbf{y}_t^o - H\mathbf{x}_t^b - \mathbf{H}_t\mathbf{U}\delta\boldsymbol{\chi}_t\right)\mathbf{R}_t^{-1}\left(\mathbf{y}_t^o - H\mathbf{x}_t^b - \mathbf{H}_t\mathbf{U}\delta\boldsymbol{\chi}_t\right)^T + \frac{1}{2}\sum_{t=1}^{T}(\delta\boldsymbol{\gamma}_t)^T(\delta\boldsymbol{\gamma}_t).$$

In this formulation, the minimization problem is simpler because the background and model error terms do not involve explicit error covariance matrices, but there is now the need to perform $\delta\mathbf{x} = \mathbf{U}\delta\boldsymbol{\chi}$ in the observation term at each iteration step. Nevertheless, this form of variational DA has become the popular approach at operational centers due to its computational cost advantages. A detailed review of the CVT approach can be found in Ref. 9.

1.2 Ensemble methods

As variational DA applications became popular at operational forecast centers in the 1990s, several weaknesses were also being recognized and can be summarized as the static (and commonly simplified) nature of the background-error covariance matrix (**B)** and the need to develop the linearized and adjoint versions of model and observation operators *M* and *H*, respectively. At around the same time, Evensen[10] proposed the ensemble Kalman filter (EnKF) as an alternative, to replace **B** with a flow-dependent covariance matrix obtained from an ensemble of model forecasts. Once running such computationally expensive ensemble forecasts becoming feasible in the 2000s, the EnKF gained popularity in DA research.[11-12] In essence, all EnKF applications are "flavors" that solve the following set of equations:

$$\mathbf{x}_t^a = \mathbf{x}_t^f + \mathbf{K}\left(\mathbf{y}_t^o - H\mathbf{x}_t^f\right),$$
$$\mathbf{K} = \mathbf{P}^f H^T\left(H\mathbf{P}^f H^T + \mathbf{R}\right)^{-1},$$
$$\mathbf{x}_{t+1}^f = M\mathbf{x}_t^a,$$

where subscripts "a" and "f" refer to analysis and forecast, respectively. **K** denotes the Kalman gain, and $\mathbf{P}^f$ represents the background-error covariance matrix. The equations are applied to both the ensemble mean and members in the same manner.

The first successful implementation of this general EnKF formulation became known as the stochastic EnKF and involved treatment of observations as random variables by explicitly perturbing them with random noise for the update of each ensemble member.[13-14] At about the same time, deterministic versions of the EnKF were proposed that did not necessitate the perturbation of observations: the ensemble square-root filter (EnSRF;[15]), the ensemble adjustment Kalman filter (EAKF;[16]), and the ensemble transform Kalman filter (ETKF;[17]).

In all of these EnKF applications, observations are assumed to be simultaneous, valid at the center of the DA time window, although they are typically collected at varying times within that window. Thus, a further generalization that involves the accounting for the time dimension can be envisioned and is known as the ensemble Kalman smoother (EnKS;[18]), where the typical EnKF update equation can be modified to account for the time evolution of the forward-calculated observations $H_t\mathbf{x}_t^f$ (three-dimensional EnKS) or the full Kalman gain that also involves the time evolution of $\mathbf{P}_t^f$ (four-dimensional EnKS), as indicated by the subscript *t*.

As with all DA applications, the EnKF and its variants bear certain limitations that cause them to deviate from the optimal-filter solution. One such limitation is the ensemble size that arises from practical restrictions due to availability of computing resources. This causes severe under-sampling in the background-error covariance matrix $\mathbf{P}^f$ that should theoretically represent the large degrees of freedom of the relevant atmospheric processes resolved in the numerical model. One popular, albeit ad-hoc, approach is known as covariance localization, which is either carried out explicitly in ensemble space or implicitly in observation space.[19] But even with covariance localization, ensemble variance is still commonly found to be insufficient due to model and observation representativeness errors that are not appropriately accounted for. Further techniques are therefore developed that aim to inflate ensemble variance explicitly through various approaches, such as additive inflation that typically adds white noise q_t to model dynamics so that $\mathbf{x}_{t+1}^f = M\mathbf{x}_t^a + q_t$, where $q_t \sim N(0, \mathbf{Q}_t)$ as before,[14] multiplicative inflation such as relaxation to prior perturbation (RTPP;[20]), and relaxation to prior spread (RTPS;[21]). A further generalized discussion of these methods can be found in Ref. 22.

1.3 Hybrid Methods

As explained in the previous two sections, both variational and EnKF methods have weaknesses that need to be circumvented, by mostly ad-hoc methods, to be successful. It therefore makes sense to somehow combine these two methods to take advantage of their strengths while minimizing their weaknesses. The earliest form of the hybrid implementation was proposed for a 3DVar application,[23] in which the background-error covariance matrix was represented as a weighted combination of a static matrix **B** and an ensemble-based matrix $\mathbf{P}^f$ as follows:

$$\mathbf{B}_{hyb} = (1-\alpha)\mathbf{P}^f + \alpha\mathbf{B},$$

where the weighting factor α ranges from 0.0 to 1.0 and its value typically depends on the application. Since the rank of $\mathbf{P}^f$ is limited by design but there is no theoretical restriction on the rank of **B**, their linear combination in this way results in a higher-rank $\mathbf{B}_{hyb}$ that is expected to partially ameliorate the issue of

sampling error encountered in pure-EnKF applications. Meanwhile, Lorenc[24] suggested to partition the analysis increment into two as follows:

$$\delta\mathbf{x} = \beta_1\delta\mathbf{x}_1 + \beta_2\delta\mathbf{x}_2,$$
$$\delta\mathbf{x}_1 = \mathbf{B}^{1/2}\mathbf{v}_1,$$
$$\delta\mathbf{x}_2 = \mathbf{P}^{f\,1/2}\mathbf{v}_2.$$

In practical terms, this is equivalent to augmenting the standard 3DVar control variables $\mathbf{v}_1$ with a new set $\mathbf{v}_2$ that represents the preconditioning based on the ensemble covariance $\mathbf{P}^f$. Wang et al.[25] later provided proof that the approaches in Refs. 22-23 are mathematically equivalent. Wang et al.[26] later applied the approach[23] in an ETKF-3DVar scheme.

It should be noted that Lorenc[27] suggested clarification to the various (and sometimes confusing) past usage of nomenclature for hybridization. This becomes especially important in 4DVar applications because the time dimension introduces a choice for whether to minimize in model space (thus requiring linear and adjoint operators as in pure 4DVar), in observation space (thus circumventing the use of linear and adjoint operators) or in dual space[63] (which also requires the liner and adjoint operators). This choice led to the appearance of the three main approaches in the last decade. Namely, hybrid 4DVar, En4DVar and 4DEnVar all utilize ensemble-based background-error covariance statistics in a 4DVar system, but hybrid 4Dvar and En4DVar maintains the linear and adjoint formulation of 4DVar while 4DEnVar replaces it with the observation-space formulation. Despite their differences, En4DVar and 4DEnVar are both known as "pure" EnVar systems. The term "hybrid", then, applies only to the further blending of the ensemble-based and static error covariances. Nevertheless, the EnVar applications in practice generally involved the additional hybrid component (e.g., Refs. 28-30).

1.4 Particle filters

As EnKF and variational DA approaches gradually evolved into hybrid-EnVar/4DVar methods, and such applications demonstrated generally superior performance to EnKF or 4DVar alone (e.g., Ref. 31), their limitations also became clear. For instance, En4DVar inherits the limitations of 4DVar in its continued reliance on linearized operators and adjoints, while 4DEnVar is naturally restricted by the accuracy of the underlying ensemble and is unable to account for advecting covariance statistics as the observation-space error term is evaluated at the initial time of the assimilation window. A common underlying thread for all of these issues is the assumptions of linearity and Gaussianity in both the EnKF and 4DVar approaches (and their hybrids by extension): the prediction problem becomes increasingly nonlinear as mesoscale and convective-scale processes are involved, resulting in increasingly suboptimal solutions in DA.

Particle filters offer distinct advantages over the EnKF and 4DVar approaches because by design they are able to operate on non-Gaussian distributions and don't require specific assumptions for underlying probability density functions (PDFs). Instead, the particle filter approximates Bayes' theorem by defining a prior (forecast) PDF as a sum of weighted individual particles that each represent a delta function. The original Bayes' theorem is defined as follows:

$$p(\mathbf{x}|\mathbf{y}) = \frac{p(\mathbf{y}|\mathbf{x})p(\mathbf{x})}{p(\mathbf{y})},$$

where $p(\mathbf{x})$, $p(\mathbf{y}|\mathbf{x})$, and $p(\mathbf{x}|\mathbf{y})$ are the prior PDF, conditional observation likelihood given the prior PDF, and posterior PDF, respectively, and $p(\mathbf{y}) = \int p(\mathbf{y}|\mathbf{x})p(\mathbf{x})d\mathbf{x}$ represents the total observation probability as the normalization factor. In the standard bootstrap particle filter, the prior PDF is then approximated by the following sum:

$$p(\mathbf{x}) \approx \frac{1}{N_e}\sum_{i=1}^{N_e} w_i^f \delta(\mathbf{x} - \mathbf{x}_i^f),$$

where N_e is the number of particles, δ represents the delta function, and the prior weights are $w_i^f = 1/N_e$. Applying the Bayes' rule to the posterior pdf then yields the posterior particle weights as follows:

$$w_i^a = \frac{p(\mathbf{y}|\mathbf{x}_i^f)}{\sum_{j=1}^{N_e} p(\mathbf{y}|\mathbf{x}_j^f)}.$$

However, as Snyder et al.[32] discussed, the standard bootstrap form of the particle filter suffers from particle weight collapse for high-dimensional applications if one of the likelihoods $p(\mathbf{y}|\mathbf{x}_i^f)$ is much larger than the rest, i.e., there is not a sufficient number of particles that sample the prior likelihood near the observation. In fact, the minimum number of particles grows exponentially with the number of state variables needed to be observed. This issue is also known as weight degeneracy.

Because of the high dimensionality of atmospheric DA applications, new methods need to be developed to avoid or minimize the impact of weight degeneracy in particle filters. As van Leeuwen et al.[3] discussed, four main approaches to this issue were developed in this area. Proposal density particle filters (e.g., Ref. 33) apply an additional proposal distribution to allow the posterior particles to become more densely concentrated near the observations. In transportation particle filters (e.g., Ref. 34), the idea is to rather define a matrix **D** that transforms prior particles directly to posterior particles, i.e., $\mathbf{X}^a = \mathbf{X}^f\mathbf{T}$, where the prior and posterior ensembles **X** are composed of N_e realizations of particles $(1/M, \ldots, 1/M)^T$ and $(w_1, \ldots, w_M)^T$, respectively, and M represents the size of the state vector. The coupling matrix is designed so that $\mathrm{T}_{ij} \geq 0$, $\sum_{i=1}^{M} \mathrm{T}_{ij} = 1/\mathrm{M}$, and $\sum_{j=1}^{M} \mathrm{T}_{ij} = w_i$. A typical application attempts to minimize the total distance between the posterior and the prior in state space. A third approach introduces the concept of localization (Refs. 35-37) that attempts to minimize the negative effects of weight degeneracy by only allowing particles to be impacted by nearby observations. However, this is not trivial because a smooth distribution of the global set of particles from a set of locally updated particles is not always guaranteed. Finally, a hybrid approach with an EnKF scheme (e.g., Ref. 38-39) or an EnVar scheme[40] can be adopted to improve the benefits of localization.

2. Overview of the Global Operational NWP Models and DA Systems

In this section, the global NWP models and DA systems for several operational centers are described. Most of these global NWP systems use horizontal resolutions ranging from ~10 to 20 km with a diverse range of vertical resolutions and provide numerical weather predictions out to 5-10 days. Of the DA systems for the global analysis, most use a form of the incremental 4DVar method.[8] Various ensemble

techniques (e.g. local ensemble transform Kalman filter (LETKF)) are used in the DA systems to account for the flow-dependent "errors of the day" for the background error covariances. For TC applications, these model upgrades (e.g. model resolutions, model physics configurations, land/ocean/wave coupling) and observation DA advancements (e.g. new model state variables, new observing platforms) contributed to the TC forecast improvements. This section is not intended to be exhaustive to list all the aspects that affect TC predictions, but simply an overview of the overall NWP system features that are relevant to TC forecasting. **Table 1** summarizes the name, horizontal and vertical resolution of the global NWP models and corresponding DA systems, including the DA technique, ensemble component, coupling status and the radiative transfer model (RTM). Note that two main RTMs (Radiative Transfer for TOVS (RTTOV); Community Radiative Transfer Model (CRTM)) are used in the listed NWP centers. **Figure 1** illustrates the typical verification conducted by the National Hurricane Center (NHC) every year. Global models are mostly used in the track verification, while regional or statistical models are verified for the intensity forecasts. Full acronyms of each model can be found at https://www.nhc.noaa.gov/verification/pdfs/Verification_2020.pdf. In general, global models have superior track forecast skill than the regional models, likely due to better representation of the large-scale environment flow from the global model, but regional and statistical models outperform their global counterparts on intensity forecasts, largely attributed to factors such as higher model resolution, better physics and convection schemes for TCs, better use of TC inner-core observations, etc., from the regional dynamic models.

Table 1: Summary of NWP Centers' global deterministic models and DA systems

Institute (Country)	Model			DA system				
	Name	Horz. res.	Vert. res.	Technique	Ensemble	Coupling	RTM	Use of TC Observations
ECMWF (Europe)	IFS	T1279co (9km)	L137 (to 0.01hPa)	Increm. 4DVar	EDA	Land, ocean, and wave	RTTOV	No use of TCvitals to relocate vortex; all-sky satellite radiance assimilation for some microwave sensors; use reconnaissance dropsondes
Met Office (UK)	Unified Model	10 km at mid-latitudes	L70 (~80km)	Hybrid Increm. 4DVar	En-4DEnVar	-	RTTOV	Uses TCvitals to initialize a vortex; uses reconnaissance dropsondes
NCEP (USA)	FV3-GFS	T1534 (13km)	L127 (~ 80km)	4DEnVar with 4D-IAU	LETKF	-	CRTM	Assimilates minimum SLP from TCvitals, but otherwise does not use vortex relocation; all-sky radiance assimilation for some MW sensors; use reconnaissance dropsondes and flight-level data
FNMOC (USA)	NAVGEM	T681 (19km)	L60 (to 0.04hPa)	Hybrid Increm. 4DVar	ET	-	CRTM	Uses TCvitals to generate synthetic observations for vortex initialization; uses reconnaissance dropsondes
JMA (Japan)	JMA-GSM	TL959 (20km)	L128 (to 0.01hPa)	Increm. 4DVar	LETKF	-	RTTOV	Uses TC bogus data to initialize a TC vortex; all-sky radiance assimilation for some MW sensors

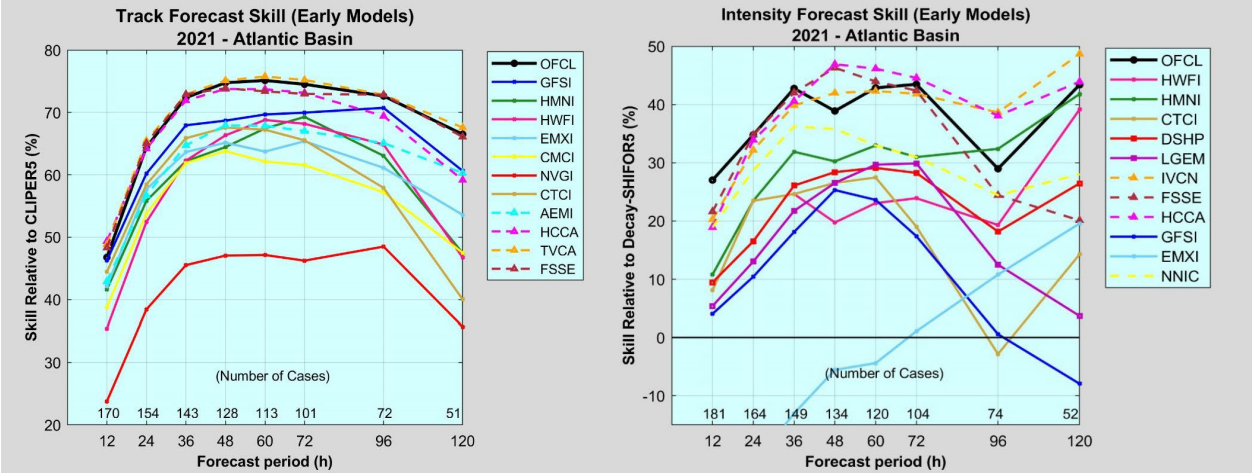

Figure 1: Preliminary 2021 hurricane season track (left) and intensity (right) forecast verification for the Atlantic Basin. Figure courtesy of Blake & Brennan.[41] The NWP operational models reviewed in this overview are EMXI (ECMWF global model), GFSI (NCEP global model), NVGI (U.S. Navy global model) and HWFI (NCEP regional model).

2.1 ECMWF

The Integrated Forecast System (IFS) contains a comprehensive Earth-system model and DA system, and has been run at the ECMWF since 2004. The spectral atmospheric model uses the efficient semi-Lagrangian semi-implicit scheme to solve the hydrostatic and the shallow-atmosphere approximations of the governing equations.[42] The IFS model in the vertical is discretized using a finite-element scheme. The IFS also introduced a reduced Gaussian grid in the horizontal, the Legendre transforms, and improvements to the model's basic architecture to further improve the computation efficiency.[43] The most recent cycle of the IFS (CY47R1) implemented in June 2020 has a native horizontal resolution of ~9 km with 137 vertical levels (up to 0.01hPa). The atmospheric DA uses a continuous long assimilation window[44] with hybrid incremental 4DVar[8] for the high resolution (HRES) deterministic forecast system, along with 51 lower resolution members for the Ensemble of Data Assimilation (EDA;[45]) that provides the perturbed initial conditions for the ensemble (ENS). The background error covariances are a linear combination of a pre-existing climatological background error covariance and a flow-dependent background error covariance inferred from the lower-resolution EDA. ECMWF also runs an ocean analysis system (OCEAN5) to provide ocean and sea-ice initial conditions for HRES and ENS. Coupled ocean and ocean wave models also provide SST, surface stress, Stokes drift and turbulent energy flux at the ocean surface. The atmosphere-ocean coupling that was introduced in the IFS cycle 45r1 on the 5 June 2018 resulted in significant improvements for TC intensity forecasts.[46]

ECMWF does not use information from the Tropical Cyclone Vitals Database (TCvitals) in its DA system or through a vortex relocation.[47] Satellite observations are the dominant data sources around tropical storm environment.[48] Various efforts have been made to improve the use of scatterometer winds,[49] expand all-sky satellite radiances from a range of microwave and infrared instruments (e.g. Ref. 50), and improve dropsonde assimilation[47] to better initialize TC analyses and forecasts.

Recent upgrades includes the introduction of single-precision for HRES and ENS to significantly reduce the arithmetic precision in many of the NWP model calculations without compromising the quality of

weather forecasts, additional TC tracks and graphical products from the 0600 and 1800 UTC forecast cycles, all-sky assimilation of AMSU-A, and improved physical basis for moist processes, etc. Cycle upgrades 47R3 implemented in October 2021 improved TC position error by 10% in HRES and ENS. The most up-to-date information can be found here: https://confluence.ecmwf.int/display/FCST/Changes+to+the+forecasting+system.

2.2 Met Office

The Met Office Unified model (UM) is designed for numerical weather prediction (ranging from a few days) to seasonal forecasting and climate (hundreds of years) modeling. The UM uses semi-lagrangian and semi-implicit formulations to solve the compressible non-hydrostatic equations of motion. The global model is configured at a horizontal resolution of 0.140625° x 0.09375° (about 10 km at mid-latitudes) with 70 vertical levels. The DA system employs a hybrid incremental 4DVar method.[30] Recent improvement of the model ENDGame (Even Newer Dynamics for General atmospheric modelling of the environment) dynamic core for accuracy, stability and scalability and increased deep entrainment rate in the convection scheme resulted in better representation of TCs in its global model.[51] Note that TCvitals are used in the DA system to initialize the vortex.[52] Reconnaissance dropsonde data, except those designated as 'eyewall' or 'rainband' data, are routinely assimilated in the DA system whenever they are available (personal communication with Heming, 2021).

In 2019, the Met Office introduced the parallel suite 43 (PS43) that provided significant upgrades to the global and ensemble systems, atmospheric physical process in the global model and an independent soil moisture assimilation (https://www.metoffice.gov.uk/services/data/met-office-data-for-reuse/ps43_aws). The global ensemble replaced the ETKF scheme to an ensemble of 4DEnVars (En4DEnVar), which is an ensemble of initial conditions (i.e. analyses) generated from their respective DA cycles. The model physics change was the first major upgrade since the implementation of ENDGame with PS34. The physics package Global Atmosphere 7.2 (GA 7.2) upgraded the deep convection, the characterization of cloud, radiation, warm rain microphysics and boundary-layer processes. Overall this change improved TC track forecasts and strike probabilities.
New development of a fully coupled forecast system including atmosphere, land, ocean and sea ice components is scheduled to be operational soon, along with a weakly coupled atmosphere-ocean DA system to better utilize observations from various earth system components. Research topics in development for operational transition can be found in https://www.metoffice.gov.uk/research/weather/research-to-operations/.

2.3 NCEP

NOAA's National Centers for Environmental Prediction (NCEP) Global Forecast System (GFS) employed a finite-volume cubed-sphere (FV3) dynamic core[53] as the Next Generation Global Prediction System (NGGPS) starting in June 2019. The operational model run at the Environmental Modelling Center (EMC) FV3-GFS v15 maintains a horizontal resolution of 13 km with 127 vertical levels extending up to 80 km. The FV3-GFS provides numerous improved physics parameterizations compared to the previous version of the GFS. The improved physics package in the FV3-GFS, particularly with the GFDL microphysics,[54] the Yonsei University (YSU) PBL scheme,[55] and a mixed-layer ocean model,[56] showed improvement in hurricane intensity prediction over all basins.[57]

The FV3-GFS v15 DA utilized the hybrid 4DEnVar algorithm[58] with heritage from the previous version of the global data assimilation system (GDAS). Several changes to the DA system were made along with the initial implementation of FV3-GFS in June 2019. These included an increase in the analysis increment and ensemble resolution, the addition of Advanced Technology Microwave Sounder (ATMS) all-sky (clear and cloud-affected) radiances, Infrared Atmospheric Sounding Interferometer (IASI) moisture channels, an upgrade to the quality control of GOES atmospheric motion vectors (AMV) and the Cross-Track Infrared Sounder (CrIS) usage, and removal of TC relocation using TCVitals (https://www.weather.gov/media/notification/scn19-40gfs_v15_1.pdf).

The FV3-GFS v16 upgrade on 22 March 2021 provides many model upgrades and DA changes (https://www.weather.gov/media/notification/pdf2/scn21-20gfs_v16.0.pdf). This is the first major upgrade to FV3-GFS since the replacement of the spectral dynamical core in June 2019. The number of model vertical levels is extended from 64 to 127 layers with a model top up to ~80 km. The model physics upgrades include better gravity wave parameterization, better representation of the PBL process using a scale-aware turbulent kinetic energy (TKE) based moist eddy-diffusivity mass-flux (EDMF) vertical turbulence mixing scheme (EDMF-TKE), and improved solar radiation in the radiation package. The new version of the hybrid 4DEnVar system adds a new 4D incremental analysis update (IAU) and replaces the Ensemble Square Root Filter with the LETKF for the ensemble covariances. Other DA changes include adding correlated observations errors for hyperspectral infrared sounders, updating the variational quality control and applying the Hilbert curve for high-density observations, and adding the assimilation of high-density flight-level wind, temperature, and moisture observations in the tropical storm environment.[59]

2.4 US Navy - FNMOC and NRL

The Navy Global Environmental Model (NAVGEM) is the U.S. Navy's global NWP model, which is developed by the U.S. Naval Research Laboratory (NRL), and is run operationally by the Fleet Numerical Meteorology and Oceanography center (FNMOC). The spectral NAVGEM model uses a semi-Lagrangian semi-implicit dynamic core with advanced physical parameterizations.[60] The current operational model is configured at a horizontal resolution of 19 km (spectral triangular truncation of T681) with 60 vertical levels up to 0.04 hPa.

The NRL Atmospheric Variational Data Assimilation System-Accelerated Representer (NAVDAS-AR)[61-62] dual-space strong-constraint 4DVar is used with NAVGEM. The operational NAVDAS-AR was upgraded in October, 2016 to include a hybrid background error covariance.[63] The hybrid background error covariances are currently a linear combination with 75% of the initial background error covariance derived from the static background error covariance and 25% derived from an 80-member flow-dependent ensemble. The ensemble members are generated using the operational ensemble forecasting system[64-65] applied at NAVDAS-AR inner loop solver resolution of T119 (~110 km). The operational ensemble is based on a local formulation of the Bishop and Toth[66] ensemble transform technique. TCvitals are used to initialize a modified Rankine vortex that is combined with the model background. From this, synthetic observations of wind profiles and surface pressure are generated for assimilation with the hybrid NAVDAS-AR.[67]

The US Navy's next generation NWP system - NEPTUNE (Navy Environmental Prediction sysTem Utilizing a Nonhydrostatic Engine[68] is currently being developed and will provide a unified system for the global and limited area applications with capabilities for multi-scale nonhydrostatic dynamics, scale-aware parameterization with static mesh refinement for limited area applications, and flexible, accurate and conservative numerical computations. The Nonhydrostatic Unified Model of the Atmosphere (NUMA;[69]) dynamic core uses a three-dimensional spectral element technique with a sphere-centered Cartesian coordinate system on the Cubed sphere. The NEPTUNE will also provide coupling with ocean, land and sea ice. The NEPTUNE data assimilation component is being developed using the Joint Center for Satellite Data Assimilation's (JCSDA) JEDI (Joint Effort for Data assimilation Infrastructure) community-supported initiative. The initial application of the NEPTUNE-JEDI system will be a global 3DVar system.[70]

2.5 JMA

The JMA Global Spectral Model (GSM) and the Global Ensemble Prediction System (GEPS) models are often used for TC information. The current GSM (GEPS) is run at about 20 km (40 km) horizontal resolution (spectral triangular truncation of TL959 and TL479, respectively) with model top at 0.01 hPa. The JMA GSM uses the incremental 4DVar approach[8] to generate initial conditions at a horizontal resolution of ~55 km. The background error covariance is a weighted average of climatological and ensemble-based background error covariances[71] and is further improved with increasing ensemble size and hybrid covariance weight.[72]

The JMA has devoted significant effort to the all-sky MW and IR radiance assimilation in the global DA system.[50,73] Initial testing of the all-sky MW radiance assimilation resulted in significant improvement of TC analyses and forecasts (Figure 5 in Ref. 50). In December 2019, JMA operational global NWP system began assimilating all-sky radiances from the MW imagers and MW water-vapor sounders.[74] For TCs over the NW Pacific, typhoon bogus data (also known as pseudo-observations) are derived empirically and then are assimilated to obtain the initial state of TCs in the model.[75] These data typically consist of the mean-sea-level pressure (MSLP) and profiles of wind vectors around TCs.

The JMA global NWP upgrade in March 2021 increased model vertical level from 100 to 128 with the model top same at 0.01 hPa and improved soil moisture analysis.[76] The JMA placed high priority in the next twenty years to improve the prediction of heavy rain and storm surges caused by typhoons, implement all-sky assimilation of microwave and infrared satellite radiances, and develop artificial intelligence (AI) technology for applications in physics parameter optimization, observation data quality control and other areas.[77] Latest activities on the NWP development can be found here: https://www.jma.go.jp/jma/en/Activities/nwp.html.

3. Overview of the Regional Models

There are a number of operational regional models that can provide skillful TC forecasts, such as COAMPS-TC system[78] run by FNMOC, TyphoonWRF (TWRF;[79-80]) run by Taiwan's Central Weather Bureau, and NCEP's Hurricane Weather Research and Forecasting (HWRF) and Hurricanes in a Multi-scale Ocean-coupled Non-hydrostatic model (HMON). Note that although TWRF uses a 3D-Var system, the TC intensity forecasts are inferior compared to the global ECMWF and NCEP models.[80] COAMPS-TC does not have an operational DA system to generate the initial vortex, but there are some ongoing research efforts to integrate COAMPS-TC with either 3D-Var, 4D-Var or ensemble system. The vortex initialization scheme in the operational COAMPS-TC uses the TC warning messages as input, in combination with initial and boundary conditions from either a GFS (abbreviated as CTCX) or a NAVGEM (abbreviated as COTC). HWRF model is one of the leading regional models with an advanced DA system, and provides more skillful intensity forecasts than the global models on average. Because of this, the HWRF model and corresponding DA specifics are discussed in great detail in this section. Also, given that a new hurricane model at NOAA – the Hurricane Analysis and Forecast System (HAFS) - is scheduled to replace both HWRF and HMON in June 2023, a brief review on HAFS is provided as well.

3.1 NCEP HWRF

The HWRF model is run on a per-storm basis with a variety of configurations depending on the basin of interest. Configurations outside the North Atlantic (NATL) and Eastern North Pacific (EPAC) use no data assimilation and are instead initialized with the NCEP GFS analysis for the large-scale environment along with an algorithm that relocates and adjusts the vortex from the previous 6-h HWRF forecast to better match the location and structure in TCVitals. In the NATL and EPAC, the relocated and adjusted 6-h HWRF vortex is inserted into the GFS 6-h forecast to provide a first-guess for 3DEnVar. The remainder of this subsection focuses on the data-assimilation configuration of HWRF.

Within the NATL and EPAC, HWRF utilizes one of two different data assimilation approaches depending on available resources (**Figure 2**). For lower priority storms that are weaker, are not threats to land, and do not have reconnaissance data, the flow-dependent covariance for 3DEnVAR is provided by the NCEP GDAS global ensemble members. While this covariance choice is suboptimal for assimilating data in the TC vortex, it nevertheless performs reasonably well for weaker TCs. For hurricanes, however, this configuration can perform poorly with short-term negative intensity bias that typically worsens as the TC intensity increases. Tong et al.[82] thoroughly described this configuration of HWRF and examined its performance with various types of reconnaissance data.

A more advanced implementation of HWRF is used for priority storms that are likely to be significant threats to land and have reconnaissance data or for stronger oceanic storms, resource permitting. This implementation of HWRF is similar to that in Lu et al.[83], wherein a cycled EnKF provides mesoscale error covariance for the variational minimization. The EnKF ensemble is run at a somewhat lower resolution than the deterministic control, and subsequent to the EnKF update, the analysis mean is replaced by the 3DVar analysis. Lu et al. [83] and Pu et al.[84] both showed that using mesoscale error covariance for 3DEnVar significantly reduces short-term negative intensity bias endemic to the legacy system where global covariance is used. Consistent results were found over a much larger sample in internal testing at EMC. A recent addition to this configuration was the inclusion of stochastic physics perturbations, which were found to increase ensemble spread and provide superior analyses and forecasts.[81]

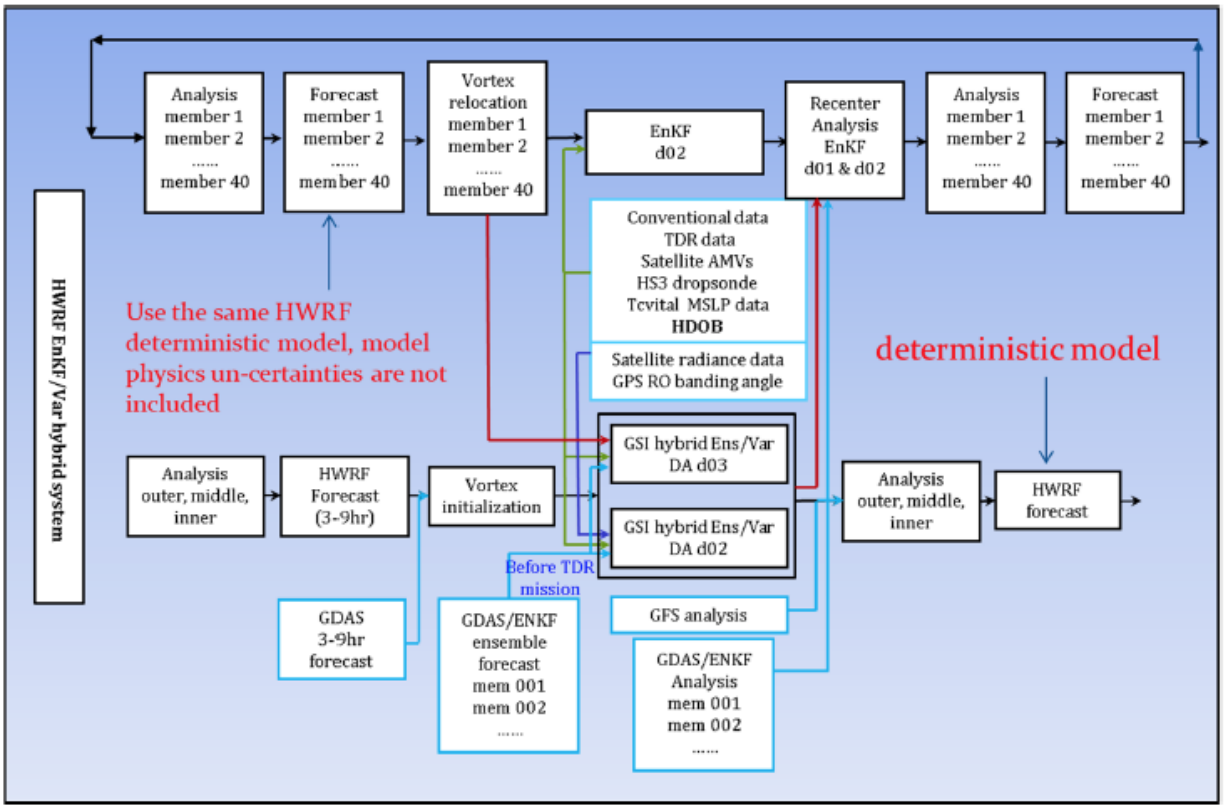

Figure 2. Workflow of the HWRF data assimilation system, adopted from Zhang et al.[81] Under the advanced configuration, all tasks are run. In the legacy configuration, the ensemble members and EnKF (top of figure) do not run.

Even with its more advanced configuration, asymmetric inner core analysis increments require further treatment in HWRF. Tong et al.[82] showed that asymmetric inner core data coverage (e.g., from reconnaissance) can cause imbalances in analysis increments, which degrade the short-term forecast with substantial negative intensity bias. Lu et al.[83] demonstrated that 3DEnVar is particularly susceptible to this problem when used with a 6-h DA window, which is current operational practice. Possible long-term solutions to this problem include using 4DEnVar or more frequently cycling 3DEnVar; both improved short-term negative intensity bias endemic to HWRF. As a stop-gap measure to combat inner-core imbalances, early versions of HWRF did not use any low-level, inner core analysis increments but instead relied on the first guess supplied by the vortex initialization procedure. In 2018 the operational HWRF employed a spectral filter to instead truncate high-wavenumber analysis increments near the inner core, which allows for much greater use of inner core reconnaissance data. Full increments are only allowed for tropical storms weaker than 50 kt. Above that intensity but below the hurricane threshold, increments with wavenumbers larger than 1 are removed from the analysis within the inner 150 km. For hurricanes only symmetric increments are allowed within 150 km. Internal testing has shown that the filter does indeed improve short-term negative intensity bias.

HWRF is the only operational model in the world to use all aircraft reconnaissance data that is transmitted in real-time (for more information on much of this data, see the next section). The aforementioned developments specifically targeting inner core data assimilation allowed for increased use of the data

compared to the initial assimilation of tail-Doppler velocity data from the NOAA WP-3D in 2013. Since that time, flight-level measurements and Stepped Frequency Microwave Radiometer (SFMR) data were added to the data that HWRF assimilates. In addition, HWRF now uses an algorithm developed at NOAA AOML that processes WMO-TEMPDROP messages to estimate the location of dropsondes (e.g., Ref. 85). This allows for more complete usage of dropsonde data in stronger TCs since dropsondes can travel several tens of kilometers in high-wind environments. In addition to reconnaissance data, HWRF makes routine use of clear-sky satellite radiances, enhanced atmospheric motion vectors, ground-based Doppler velocity, and other conventional observations used at many national centers (see Tong et al.[82] for more information). Largely as a result of improving data assimilation, HWRF now produces some of the most skillful operational model tropical cyclone intensity forecasts in the NATL and EPAC.

3.2 NCEP HAFS

Developed under a unified global and regional modeling framework, known as the Unified Forecast System (UFS) framework, HAFS is NOAA's next-generation atmosphere-ocean-wave coupled, multi-scale, high-resolution regional model system with TC-following moving nests and TC inner-core DA. HAFS is developed based on FV3 modeling system to provide TC prediction on track, intensity, storm size, and other TC related guidance (e.g. rainfall, tornado, storm surge). HAFS is planned to have the initial operational capability (IOC) ready for the 2023 hurricane season, replacing current operational hurricane prediction systems, HWRF and HMON.

Development on HAFS data assimilation began in the fall of 2021, and testing continues towards the IOC. As of the writing of this manuscript, the HAFS IOC will likely function similarly to the implementation of HWRF for "low priority" storms. That is, covariance for 3DEnVar will be provided by NCEP GDAS. HAFS uses significantly more computational resources than HWRF, and an advanced implementation with a cycled EnKF cannot be afforded for the IOC. Nevertheless, developmental testing shows that HAFS has commensurate intensity skill and superior track skill to HWRF, likely owing to improved model physics and an improved dynamic core. Current plans include two different implementations of HAFS with slightly different physics and different implementations of the vortex initialization procedure that precedes data assimilation.

Unlike HWRF, HAFS has been designed with the flexible capability to explore other options for data assimilation. Future implementations will certainly use a cycled EnKF, likely in a configuration cycled over an entire basin. Such a configuration will allow for superior treatment of satellite radiance data, and all-sky radiance assimilation is currently being explored in experimental versions of HAFS. Also being explored is superior treatment of error covariance with 4DEnVar, a multi-scale technique being developed by the University of Oklahoma, and more frequent cycling of the analysis.

4. TC Observations

The lack of direct observations in and around TCs remains one of the main challenges for accurately analyzing the vortex structure with data assimilation. The common conventional observations (**Table 2**, not intended to be exhaustive) assimilated in many operational models are generally insufficient for the task. In fact, there are often very few conventional observations available for TCs over the open ocean. Other specialized data, such as high-resolution reconnaissance observations for TCs within the range of

aircraft or Uncrewed Airborne Systems (UASs), or ground-based radars for TCs close to the coast, are extremely helpful but often not available. For that reason, operational models that need to capture the initial vortex intensity often resort to some form of artificial initialization as a preprocessing step (e.g, Tong et al.,[82]) before data assimilation. Such initialization schemes often introduce their own set of problems, and as such, it would be desirable to diminish their use in the future. The emerging use of other data types, such as rapid-scan AMVs and all-sky radiances are a few examples that could supplement reconnaissance and ground-based radar for superior analysis of TC vortices. These additional data types will be discussed in the following sections.

Table 2: Summary of conventional observation types. Acronyms in the table include Meteorological Aerodrome Reports (METAR), Coastal-Marine Automated Network (C-MAN), Pilot Balloon (PIBAL), Aircraft En-route Report (AIREP), Aircraft Meteorological Data Relay (AMDAR), Meteorological Data Collection and Reporting System (MDCRS), Tropospheric Airborne Meteorological Data Reporting (TAMDAR), Velocity Azimuth Display (VAD), Global Navigation Satellite Systems (GNSS) Radio Occultation (RO).

Conventional type	**Description**
Surface Land (METAR and Synoptic)	Surface wind, temperature, humidity, and pressure over land
Surface marine (ship, buoy, C-MAN, tide gauge)	Surface wind, temperature, humidity, and pressure over water or coastal regions
Rawinsonde, dropsonde	Upper air wind, temperature, humidity, and pressure measured from rawinsondes
PIBAL	Upper air wind from pilot balloons
AIREP, AMDAR, MDCRS, TAMDAR	Upper air wind, temperature, humidity, and pressure measured from aircraft
VAD winds	Upper air winds estimated from Doppler radar (velocity azimuth display)
AMV winds	Atmospheric Motion vectors: tropospheric winds estimated from tracking clouds or water vapor features in successive satellite imagery
Scatterometer winds	Ocean surface winds estimated from scatterometer backscatter
Ocean surface winds	Ocean surface winds from microwave radiometers
GNSS-RO	Radial occultation or refractivity
GNSS path delay	Total zenith delay and/or total precipitable water
TCVitals	TC center location, intensity, and minimum sea level pressure

4.1 Reconnaissance

Inner-core reconnaissance missions in the North Atlantic and Eastern North Pacific basins typically use Air Force Reserve C-130 (low to medium altitude) and NOAA WP-3D (low to medium altitude) aircraft to collect critical observations of the location, strength, and structure of the TC circulation, while the environmental sampling near the TC is typically achieved by the NOAA G-IV aircraft (high altitude). These aircraft are equipped with a variety of instruments that sample the wind, temperature, moisture, pressure, precipitation, and ocean surface and subsurface temperature, current, and wave fields within and

around TCs (e.g., flight-level measurements, dropsondes, airborne Doppler radar, SFMR, lower-fuselage radar, and airborne expendable bathythermographs/current profilers). NOAA and NASA teamed together in recent years to use UAS to collect TC observations.[86-89] UAS such as the Global Hawk can sample the TC up to 24 hour at an altitude of 60,000 ft (~18 km), providing not only dropsonde observations, but also remotely-sensed radar, microwave, and infrared observations.[86,90-92]

Tropical cyclones in other oceanic basins are occasionally observed by reconnaissance missions, such as those from the Observing System Research and Predictability Experiment (THORPEX) Pacific Asian Regional Campaign (T-PARC;[93]) and the Dropsonde Observations for Typhoon Surveillance near the Taiwan Region (DOTSTAR;[94]), where dropsondes observations were the primary datasets.

The assimilation of dropsonde data has long been known to provide beneficial impact for TC track forecasts. For example, Ditchek et al.[95] reviewed the results from 30 papers starting from the early 1990s and found that dropsonde assimilation alone has improved track forecasts by about 10% on average. This paper also presented an ongoing multi-year assessment of dropsonde impact using the basin-scale version of the 2020 HWRF. The study authors found a track improvement of up to 5%, which is a bit lower than previous large-scale studies. This might mean that the dropsondes have less of an effect on track errors as the use of other data sources (e.g., from satellites) increases.

However, other reconnaissance data is also beneficial for reducing TC track errors. Weng & Zhang[96] published the first large (e.g., 100s of cases) assessment of the impact of inner-core DA with a research system. They found that track forecasts improved by 10-15% when flight-level data and dropsondes were assimilated. In another study with a large number of test cases, Tong et al.[82] used the 2013 version of HWRF, and found that TDR, SFMR, and flight-level data improved TC track forecasts by roughly 10%. More recently, in preparation for the 2021 GFS upgrade, NCEP found a 5-10% improvement in TC track forecasts when flight-level reconnaissance observations were assimilated (personal communication with Daryl Kleist). This shows that even with the expanding data availability from other sources, improving the use of reconnaissance observations can still benefit track forecasts.

A growing body of work also shows reconnaissance data can improve TC intensity forecasts. In their composite assessment, Ditchek et al.[95] found that dropsondes alone improve intensity by up to 10%. Weng & Zhang[96] similarly found that dropsondes and flight-level observations improve intensity forecasts by around 10%. Meanwhile, Aberson et al.[97] found in their research system HEDAS[98-99] that the combination of TDR, SFMR, and flight-level data improved intensity forecasts over 20% in cycles with TDR data present. Finally, though Tong et al.[82] found that assimilating reconnaissance data degraded short-term hurricane intensity forecasts due to significant deficiencies in HWRF physics and data assimilation, on average the additional data improved forecasts by up to 20% after 24h.

Recent research suggests there is significant potential for further improvements of operational TC intensity forecasts through the assimilation of reconnaissance observations. An internal assessment at NCEP used a pre-implementation version of the 2019 HWRF to examine the combined impact of all reconnaissance data for high-impact TCs from 2016-18 (e.g., Matthew, Harvey, Irma, Maria, Florence, and Michael). Even though all of these storms were of Category 4-5 intensity during the period of reconnaissance, the impact of reconnaissance DA improved the intensity forecast by ~10% (**Figure 3** in Ref. 100). This represents a notable improvement upon the results of Tong et al.[82] for hurricanes (albeit

with different storms), owing to major advances in HWRF physics, dynamics, and DA. The ongoing assessment of dropsonde assimilation impact in Ditchek et al.[95] also suggests that the impact of inner-core DA continues to improve as the HWRF DA system matures.

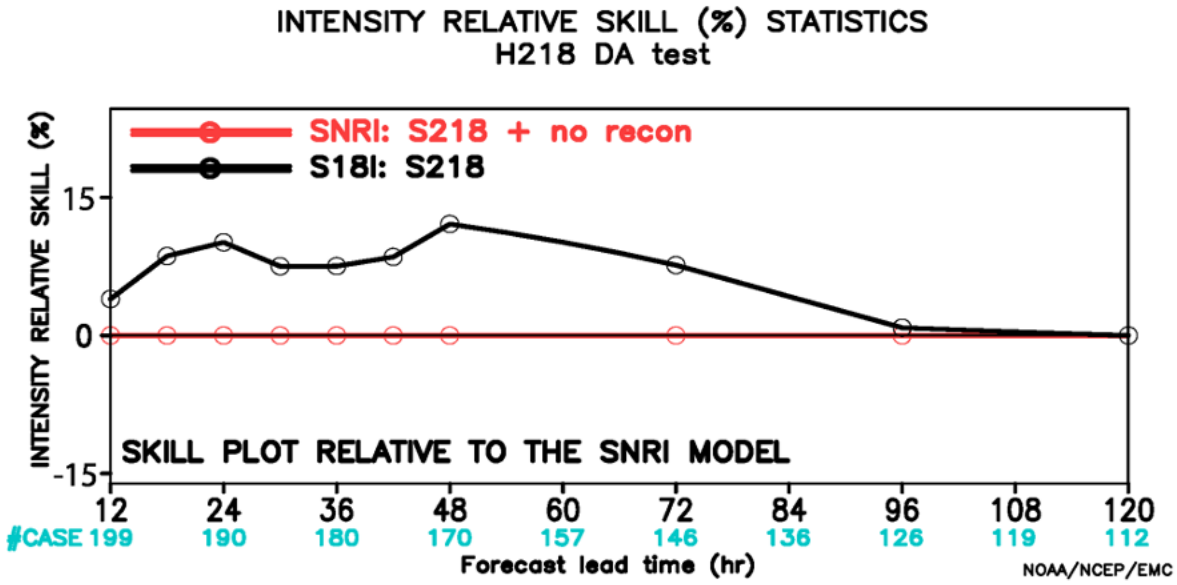

Figure 3. The impact of reconnaissance data on the operational HWRF model intensity forecasts of high-impact storms of the 2016-2018 hurricane seasons, as shown in Zawislak et al.[100] Results are expressed in terms of relative skill, where the baseline (red) is the configuration without reconnaissance data.

4.2 Ground-based radar

When TCs are sufficiently near land, ground-based radar can provide high spatial and temporal observations to supplement those of reconnaissance. Zhang et al.[101] was the first study to assess the impact of ground-based Doppler velocity for a tropical cyclone. They found that forecasts initialized without assimilating data from the US WSR-88D network failed to capture the genesis and rapid intensification of landfalling Hurricane Humberto (2007). However, when Doppler velocity data was assimilated with an EnKF, subsequent forecasts showed a landfalling hurricane of approximately the correct intensity. A number of subsequent studies explored the use of Doppler velocity from ground-based radars to improve TC forecasts around the world (e.g., Refs. 102-107).

NCEP capitalized on the WSR-88D network for operational hurricane forecast improvement beginning in 2020, when assimilation of Doppler velocity was implemented into HWRF. Internal testing at NCEP showed a roughly 10% improvement in intensity forecasts near land as a result of this improvement. Despite this advancement, a great deal more can be achieved with further use of ground-based radar. For example, NCEP does not receive radar data from anywhere outside the US (e.g., Caribbean nations, Bahamas, etc), which could be extremely beneficial for improving forecasts of near-land tropical cyclones. This potential remains an area of active research.

Recent studies show that the assimilation of ground-based radar radial velocity in combination with the reflectivity data is complementary and can further improve the model analyses and forecasts than assimilating one data type alone,[108-109] although there are various approaches to assimilate radar reflectivity data in either variational[108-110] or ensemble framework,[111] or through latent heat nudging using a digital filter.[112] In a case study of Hurricane Isabel (2003) using the 3DVar method, Zhao & Jin[109] demonstrated that the assimilation of radar reflectivity improved TC rainbands intensity and coverage, while radar radial velocity assimilation improved TC intensity and dynamic structure. The combined assimilation of radar radial velocity and reflectivity led to the best forecasts, particularly improved 24-hr precipitation forecasts along the path of the inner core during landfall.

4.3 Enhanced satellite-derived atmospheric motion vectors (AMVs)

AMVs are derived from successive multispectral geostationary satellite images by tracking the motions of clouds and water vapor structures to provide estimates of tropospheric winds. They are routinely derived using 'full-disk' images by automated processing algorithms at the operational satellite data processing centers around the globe at hourly intervals. The dynamic information provided by AMVs over conventionally-sparse regions of the globe such as the Tropics was shown to improve numerical model TC forecasts in the 1990's [167-168] and AMV data quality and quantities have improved ever since then.[114-115] For example, GOES AMVs derived from a new nested-tracking algorithm developed at NOAA/NESDIS[113] provide higher spatial and temporal resolution and better quality compared to the AMVs derived from the heritage algorithm. It has been shown these data currently available in the NCEP operational data stream can improve HWRF track forecasts.[116]

In addition to AMVs currently available in the operational stream, a recent development that could profoundly impact the initialization of TCs in the absence of reconnaissance data is the increased availability of AMVs derived from rapid-scan imagery. As described in Stettner et al. [169], more frequent image scanning along with processing methodologies designed to increase the spatiotemporal coverage of AMVs over the TC cloud canopy allows for drastically improved depictions of the smaller-scale flow fields, especially over the inner core of the storm. An example of this coverage provided by the GOES-16 satellite is shown in **Figure 4**. Similar capabilities exist from the Himawari and Meteosat satellites.

Recent studies have shown that assimilating these additional enhanced AMV datasets can have large impacts on TC intensity and structure forecasts. Using rapid-scan AMV datasets derived from GOES-16, Zhang et al. [117] and Velden et al.[118] showed improved TC intensity forecasts by 5-10% in earlier versions of the HWRF model. Results with a more recent version of HWRF show that the enhanced AMVs can also reduce track errors by roughly 10%.[119] Lewis et al. [170] discuss DA tactics for the use of the enhanced AMV observations to optimize initial analysis impact.

A limitation of the aforementioned studies using HWRF is endemic to HWRF itself. The model is not configured in a manner that can fully capitalize on the benefits of higher temporal and spatial resolution of the new AMV datasets. One example of such a limitation is that the operational HWRF is hard-coded with 6-hourly cycling, which limits the ability to effectively use high-frequency data. That being said, the next-generation HAFS that is being developed by NCEP in conjunction with numerous outside partners will provide much more flexibility to take advantage of these newly emerging datasets. Thus, in the future, the positive impact of this data should increase.

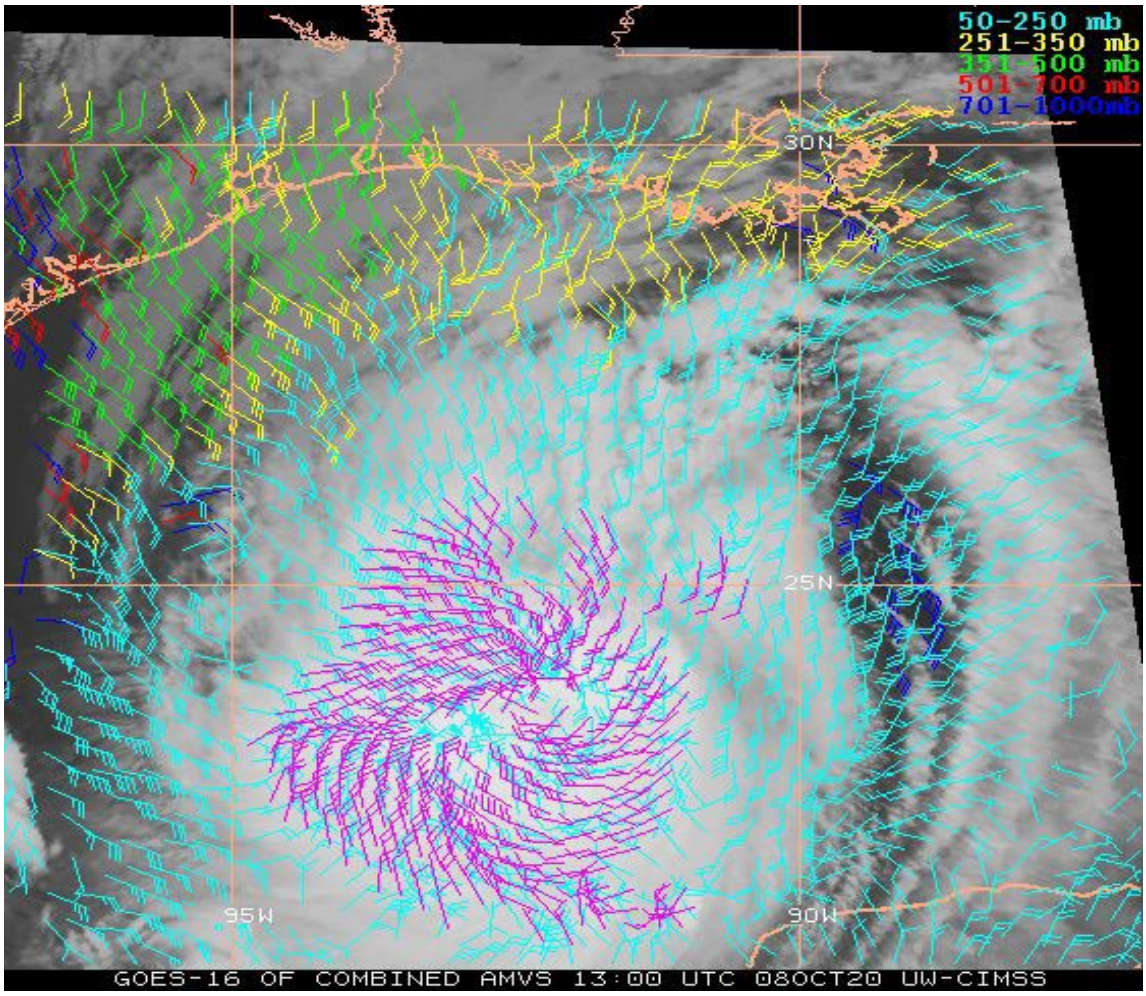

Figure 4: An enhanced AMV field over Hurricane Delta (2020) derived from GOES-16 meso- sector rapid-scan imagery. Inner-core-top vectors (50-150 mb) in magenta. Figure courtesy of C. Velden (UW-CIMSS).

4.4 All-sky satellite radiances

All-sky satellite radiance assimilation in the global models has advanced significantly over the past decades. The all-sky satellite radiance assimilation utilizes radiances not only from clear-sky measurements, but also from cloud and precipitation-affected measurements. ECMWF pioneered the implementation of all-sky radiance assimilation for the Special Sensor Microwave/Imager Sounder (SSM/IS) and the Advanced Microwave Scanning Radiometer for the Earth Observing System (AMSR/E) in 2009.[120] Since then, ECMWF has continued development of all-sky radiance assimilation to include additional microwave imagers and sounders, and extend to infrared polar-orbiting sounders and geostationary imagers.[50,121] All-sky radiance assimilation has been shown to contribute greatly to improved forecasts of dynamic quantities and precipitation beyond day 6.[122] Other operational centers such as NCEP,[123-125] Met Office,[126] JMA,[127] and Environment and Climate Change Canada (ECCC)[128] have also devoted significant efforts to expand the radiance assimilation beyond only clear-sky conditions. Global improvements to the temperature, humidity and wind fields from the all-sky radiance assimilation could directly benefit TC analyses and prediction through the assimilation of the additional

radiance information within the cloudy and precipitating areas. One study[127] shows a more pronouncement beneficial impact on TC predictions in the early and developing stages of the TC than steady and decaying stages of the TC. Regional assimilation of all-sky radiances generally presents a different challenge (e.g. domain size, model top, bias correction, etc.) compared to the global assimilation; however, several demonstration studies show the feasibility of the all-sky microwave assimilation in the regional models, and overall results in positive impacts on TC track, intensity, storm structure and precipitation forecasts.[129-132]

The extension to all-sky infrared radiance assimilation is an on-going active area of research. Chevallier and Lopez[133] identified that cloud-affected satellite radiances at 4.5, 6.3 and 14.3 μm can be directly assimilated in the DA system, similar to microwave humidity sounding channels. In particular, there is considerable interest to directly assimilate infrared radiances from geostationary imagers in cloud-resolving models for TC applications.[134] A case study by Zhao et al.[135] for Hurricane Patricia (2015) demonstrated that geostationary IR radiances can observe the multiscale structures of TCs. Additional case studies by Honda et al.[136] and Minamide & Zhang[137] demonstrated the all-sky infrared radiance assimilation from Himawari-8 can improve the TC intensity forecasts, particularly the rapid intensification forecasts. Similar case studies by Minamide & Zhang[138] and Zhang et al.[139] found that the assimilation of only channel 8 (water vapor) from the GOES-16 Advanced Baseline Imager can produce very accurate forecasts of the rapid intensification of Hurricane Harvey (2017).

5. Recent TC DA Advancements and Future Challenges

While increased model resolution and more sophisticated physics parameterization certainly promote better TC forecasts, they also bring challenges to the DA system, as the standard assumptions for model representativeness, the forward model errors, background errors, and dynamical balance constraint in the analysis may be invalid when the DA system has to ingest high spatiotemporal observations within and around TCs.

5.1 Treatment of observation error

The representativeness and forward model errors are usually considered in DA in terms of observation errors. For large first guess departures often seen in dropsondes near the core of a TC in the HRES incremental 4DVar system, Bonavita et al.[47] proposed to use ensemble DA to adaptively estimate the observation errors. This adaptive observation error model reduced the observation influence in the variational update, improved the minimization convergence and validated the bounds of the validity of the tangent linear model. The use of the adaptive error model for the dropsonde observations also led to a better position analysis and more axisymmetric and realistic structure of the TC.

For satellite radiances over the cloud and precipitation-affected areas such as TC, different shape, intensity or location of the clouds resolved in the model versus in the observations usually leads to non-Gaussian behavior (e.g. the error increases with cloud amount). The typical approach for all-sky radiance assimilation at most operational centers is to use observation error inflation.[140] A number of studies for TC all-sky microwave radiances DA employing similar error model formulations[129-132] suggested positive impacts on TC predictions. A similar observation error model to account for the cloud amount for the direct assimilation of all-sky infrared radiances was developed as well.[141] However, this error model may

not perform well in the situation when the error distribution of the first guess departures becomes two-dimensional by the mismatch of clouds in the model and in the observations.[142] In this case, the symmetric error model by Geer & Bauer[140] would still prescribe a large error for the observation even when the model and the observation agrees (on the diagonal of the two-dimensional error distribution). Presumably, it should constrain the small first guess departure by reducing the error on the diagonal of the two-dimensional error distribution. In part to overcome this, Minamide & Zhang[143] proposed a flow-dependent adaptive observation error inflation (AOEI) using the first guess departures and applied to the assimilation of GOES-R all-sky radiances for TC in an observing system simulation experiment (OSSE). The AOEI approach resulted in less root-mean-square errors (RMSEs) for some of the cloud-affected state variables at larger scales, and were better at maintaining the flow balance. However, as both observation error inflation methods are empirical, it is worth investigating whether there are more optimal or correct ways to describe the observation error (e.g. Ref. 144), particular for the TC environment.

5.2 Treatment of background error

Over the last decade, most operational centers adopted an ensemble component to incorporate into their DA systems for flow-dependent background error covariance estimates.[30, 63,135] The Met Office, FNMOC and NCEP all use hybrid background error covariance in their operational global systems. ECMWF uses the EDA to directly diagnose the background errors. Bonavita et al.[47] showed that with increased resolution, EDA may introduce small scale contributions that affect the subsequent analyses and forecasts, and result in unrealistic analyses for TCs. The study suggested that the non-Gaussian error distribution of an EDA forecast ensemble with increased resolution directly caused a multimodal TC position distribution. A solution was to reduce the resolution of the EDA-derived background errors on a linear reduced Gaussian grid together with non-homogeneous wavelet-based noise filter. Chen & Snyder[146] showed that short DA cycles may also help alleviate the large non-Gaussian forecast errors from vortex position spread.

Additionally, limited ensemble size in the ensemble-based DA requires covariance localization to counteract the sampling errors. Small ensembles can introduce a noisy background error covariance estimate, which in turn makes the analysis inaccurate.[147] Poterjoy et al.[148] demonstrated in experiments, with ensemble size ranging from 30 to 300, that the sampling differences can dominate variations of the TC outer core wind and pressure fields up to 3 days in forecast lead time. An ensemble with 60 or more members suggested a similarly realistic TC structure and sample correlations between the model state variables. Using the optimal linear filtering theory, Ménétrier et al.[149] revealed that the optimal value of the localization length may be determined by the ensemble size.

5.3 Use of new observations

Aside from the observations thoroughly discussed in section 4, there are many observations that arise from new satellite platforms, new channels from existing satellite sensors, new space-borne radar, and many other sources. For example, JMA mesoscale system has been assimilating a space-borne radar GPM/Dual-frequency Precipitation Radar (DPR) to improve TC initial conditions,[150] though improvement on the background flow-dependence and microphysics scheme was needed in order to maximize the benefits of such high-frequency observations. Lightning data from the World Wide Lightning Location Network (WWLLN) around hurricanes or typhoons has been shown to improve TC intensity forecasts.[151]

Though HWRF/GSI now has the capability to assimilate lightning data from the GOES Geostationary Lightning Mapper (GLM),[152] their impact on TC forecasting is yet to be assessed. Another new data source - Airborne Doppler wind lidar (DWL;[153-154]) has also been shown to complement TDR observations[154] and its assimilation improved TC forecasting.[154-155] Finally, observations collected from uncrewed aircraft systems (UASs) is a new area of research that shows promise to improve TC analyses and forecasts.[86-87,90,156-157]

5.4 Development of new DA methods

As we further develop the capability to simultaneously assimilate a broad network of observations that resolve different scales, a multi-scale DA method is needed. Zhang et al.[101] introduced successive covariance localization (SCL) with a sequential ensemble Kalman filter for a case study of Hurricane Humberto (2007) with dense radar observation assimilation. The filter assimilated groups of observations separately using different localization length scales. This allowed the designated groups of observations to update the prior only for the specified scales rather than for all resolved scales. Using this approach, the SCL was able to account for the presence of both the large- and small-scale errors. When this technique was applied including the assimilation of dense coastal radar observations, not only were the position and intensity forecasts for Hurricane Humberto improved, but the rapid intensification of the storm was better predicted, as compared to the no DA experiment or the experiment with a 3DVar method. Recently, scale-dependent localization (SDL) has been developed for the EnVar DA system[158-159] and ensemble-based system.[160] Multiscale-aware scheme allows the simultaneous update at all scales through the assimilation of all available observations independently at once, which not only proves to be more computational efficient and scalable, but also can lead to more accurate tropical cyclone forecasts.[159]

In parallel with the spatial scale considerations, moist physical processes and unbalanced flows, nonlinearity and non-Gaussianity at convective scales should be considered in the DA design as well. It remains an active research topic whether nonlinear DA such as particle filters,[161] or modifications to hybrid and ensemble methods to deal with non-Gaussianity,[162-163] or combination of machine learning (ML) and DA,[161,164] will be sufficient for TC DA. There are also new applications that tackle the issue that serial DA updates do not provide a unique solution because of localization. As Steward et al.[165-166] argue, in highly nonlinear regimes such as the TC inner core, this potentially becomes an important issue. Further, as the model is developed to be coupled with the ocean and by doing so has shown benefit in TC forecasting,[46] the corresponding DA system should be coupled with the ocean as well.

Author contributions

A.A. wrote the first section and provided general edits throughout the document. J.S. wrote the third section about the regional modelling and data assimilation, as well as part of the TC observations. H.C. wrote the second section about the global modeling and data assimilation, parts of the TC observations and last section. N.B. provided edits and comments throughout the document. All authors approved the final version of the manuscript.

Competing interests

The authors declare no competing interests.

Acknowledgments

We would like to acknowledge editors Prof. Luis Gimeno and Dr. Douglas Braaten for the invitation to write this review. We also sincerely thank Dr. Chris Velden and another anonymous reviewer, whose comments and suggestions have significantly improved the quality of the review article.

References

1. Bannister, R. N., 2017. A review of operational methods of variational and ensemble-variational data assimilation. *Quarterly Journal of the Royal Meteorological Society*, **143**, 607–633, doi:10.1002/qj.2982.
2. Houtekamer, P. L., & Zhang, F. 2016. Review of the Ensemble Kalman Filter for Atmospheric Data Assimilation. *Monthly Weather Review*, *144*(12), 4489–4532. https://doi.org/10.1175/MWR-D-15-0440.1
3. van Leeuwen, P. J., H. R. Künsch, L. Nerger, *et al.* 2019. Particle filters for high-dimensional geoscience applications: A review. *Quarterly Journal of the Royal Meteorological Society*, **145**, 2335–2365, doi:10.1002/qj.3551.
4. Lorenc, A. C., 1986. Analysis methods for numerical weather prediction. *Quarterly Journal of the Royal Meteorological Society*, **112**, 1177-1194, doi:10.1002/qj.49711247414.
5. Talagrand, O. and P. Courtier, 1987. Variational assimilation of meteorological observations with the adjoint vorticity equation. I: Theory. *Quarterly Journal of the Royal Meteorological Society*, **113**, 1311-1328, doi:10.1002/qj.49711347812.
6. Thépaut J.-N. and P. Courtier, 1991. Four-dimensional variational data assimilation using the adjoint of a multilevel primitive-equation model. *Quarterly Journal of the Royal Meteorological Society*, **117**, 1225–1254, doi:10.1002/qj.49711750206.
7. Trémolet Y., 2006. Accounting for an imperfect model in 4D-Var. *Quarterly Journal of the Royal Meteorological Society*, **132**, 2483–2504, doi:10.1256/qj.05.224.
8. Courtier, P., J.-N. Thépaut, A. Hollingsworth, 1994. A strategy for operational implementation of 4D-Var, using an incremental approach. *Quarterly Journal of the Royal Meteorological Society*, **120**, 1367– 1387; doi:10.1002/qj.49712051912.
9. Bannister R. N, 2008. A review of forecast error covariance statistics in atmospheric variational data assimilation. II: Modelling the forecast-error covariance statistics. *Quarterly Journal of the Royal Meteorological Society*, **134**, 1971–1996, doi:10.1002/qj.340.
10. Evensen, G. 1994. Sequential data assimilation with a nonlinear quasi-geostrophic model using Monte Carlo methods to forecast error statistics. *Journal of Geophysical Research*, *99*(C5). https://doi.org/10.1029/94jc00572
11. Houtekamer, P. L. & Mitchell H. L. 2001. A sequential ensemble Kalman filter for atmospheric data assimilation. *Monthly Weather Review*, **129**, 123–137.
12. Evensen G., 2003. The ensemble Kalman filter: theoretical formulation and practical implementation. *Ocean Dynamics*, **53**, 343–367, doi:10.1007/s10236-003-0036-9.
13. Houtekamer, P. L. and H. L. Mitchell, 1998. Data assimilation using an ensemble Kalman filter technique. *Monthly Weather Review*, **126**, 796–811.
14. Houtekamer, P. L. and H. L. Mitchell, 2005: Ensemble Kalman filtering. *Quarterly Journal of the Royal Meteorological Society*, **131**, 3269–3289, doi:10.1256/qj.05.135.
15. Whitaker, J. S., and T. M. Hamill, 2002. Ensemble data assimilation without perturbed observations. *Monthly Weather Review*, **130**, 1913–1924.

16. Anderson, J. L., 2001. An ensemble adjustment Kalman filter for data assimilation. *Monthly Weather Review*, **129**, 2884–2903.
17. Bishop, C. H., B. J. Etherton, and S. J. Majumdar, 2001. Adaptive sampling with the ensemble transform Kalman filter. Part I: Theoretical aspects. *Monthly Weather Review*, **129**, 420–436, doi:10.1175/1520-0493(2001)129,0420:ASWTET.2.0.CO;2.
18. Evensen G. 2007. Data Assimilation, The Ensemble Kalman Filter. Springer-Verlag: Berlin, 332 pp.
19. Hunt, B. R., E. J. Kostelich, and I. Szunyogh, 2007. Efficient data assimilation for spatiotemporal chaos: A local ensemble transform Kalman filter. *Physica D*, **230**, 112–126, doi:10.1016/j.physd.2006.11.008.
20. Zhang, F., C. Snyder, and J. Sun, 2004. Impacts of initial estimate and observation availability on convective-scale data assimilation with an ensemble Kalman filter. *Monthly Weather Review*, **132**, 1238–1253.
21. Whitaker, J. S., and T. M. Hamill, 2012. Evaluating methods to account for system errors in ensemble data assimilation. *Monthly Weather Review*, **140**, 3078–3089, doi:10.1175/MWR-D-11-00276.1.
22. Duc, L., K. Saito, and D. Hotta, 2020. Analysis and design of covariance inflation methods using inflation functions. Part 1: Theoretical framework. *Quarterly Journal of the Royal Meteorological Society*, **146**, 3638– 3660; doi:10.1002/qj.3864.
23. Hamill, T. M. and C. Snyder, 2000. A hybrid ensemble Kalman filter-3D variational analysis scheme. *Monthly Weather Review*, **128**, 2905–2919.
24. Lorenc, A. C., 2003. The potential of the ensemble Kalman filter for NWP - a comparison with 4D-Var. *Quarterly Journal of the Royal Meteorological Society*, **112**, 3183-3203, doi:10.1256/qj.02.132.
25. Wang, X., C. Snyder, and T. M. Hamill, 2007. On the theoretical equivalence of differently proposed ensemble-3DVAR hybrid analysis schemes. *Monthly Weather Review*, **135**, 222–227, doi:10.1175/MWR3282.1.
26. Wang, X., D. M. Barker, C. Snyder, *et al*. 2008. A hybrid ETKF-3DVAR data assimilation scheme for the WRF model. Part I: Observing system simulation experiment. *Monthly Weather Review*, **136**, 5116–5131, doi:10.1175/2008MWR2444.1.
27. Lorenc, A. C. 2013. Recommended nomenclature for EnVAR data assimilation methods. Research Activities in Atmospheric and Oceanic Modelling, A. Zadra, Ed., WCRP Report No. 10/2013, Section 1, 7-8, http://bluebook.meteoinfo.ru/uploads/2013/documents/sections.html.
28. Liu, C., C. Xiao, and B. Wang, 2008. An ensemble-based four-dimensional variational data assimilation scheme. Part I: Technical formulation and preliminary test. *Monthly Weather Review*, **136**, 3363-3373, doi:10.1175/ 2008MWR2312.1.
29. Zhang, M. and F. Zhang, 2012. E4DVar: Coupling an Ensemble Kalman Filter with Four-Dimensional Variational Data Assimilation in a Limited-Area Weather Prediction Model. *Monthly Weather Review*, **140**, 587–600, doi:10.1175/ MWR-D-11-00023.1.
30. Clayton, A. M., A. C. Lorenc, and D. M. Barker, 2013. Operational implementation of a hybrid ensemble/4D-Var global data assimilation system at the Met Office. *Quarterly Journal of the Royal Meteorological Society*, **139**, 1445-1461, doi:10.1002/qj.2054.
31. Buehner, M., P. L. Houtekamer, C. Charette, *et al*. 2010. Intercomparison of variational data assimilation and the ensemble Kalman filter for global deterministic NWP. Part II: One-month experiments. *Monthly Weather Review*, **138**, 1567–1586, doi: 10.1175/2009MWR3158.1.

32. Snyder, C., T. Bengtsson, P. Bickell, J. Anderson, 2008. Obstacles to High-Dimensional Particle Filtering. *Monthly Weather Review*, **136**, 4629–4640, doi:10.1175/2008MWR2529.1.
33. Snyder, C., T. Bengtsson, and M. Morzfeld, 2015. Performance Bounds for Particle Filters Using the Optimal Proposal. *Monthly Weather Review*, **143**, 4750–4761, doi:10.1175/ MWR-D-15-0144.1.
34. Reich, S., 2013. A nonparametric ensemble transform method for Bayesian inference. *SIAM Journal on Scientific Computing*, **35**, A2013–A2024, doi:10.1137/130907367.
35. Farchi, A. and M. Bocquet, 2018. Review article: Comparison of local particle filters and new implementations. *Nonlinear Processes in Geophysics*, **25**, 765–807, doi:10.5194/npg-25-765-2018.
36. Poterjoy, J. 2016. A localized particle filter for high-dimensional nonlinear systems. *Monthly Weather Review*, 144, 59–76, https://doi.org/10.1175/MWR-D-15-0163.1.
37. Poterjoy, J., Wicker L., and Buehner M. 2019. Progress toward the application of a localized particle filter for numerical weather prediction. *Monthly Weather Review*, **147**, 1107–1126, https://doi.org/10.1175/MWR-D-17-0344.1.
38. Stordal, A. S., H. A. Karlsen, G. Nævdal, G, H. S. Skaug, and B. Vallés, 2011. Bridging the ensemble Kalman filter and particle filters: the adaptive Gaussian mixture filter. *Computers & Geosciences*, **15**, 293–305, doi:10.1007/s10596-010-9207-1.
39. Frei, M. and H. R. Künsch, 2013. Bridging the ensemble Kalman and particle filters. *Biometrika*, **100**, 781–800, doi:10.1093/biomet/ast020.
40. Potthast, R., A. Walter, and A. Rhodin, 2019. A Localized Adaptive Particle Filter within an Operational NWP Framework. *Monthly Weather Review*, **147**, 345–362, doi:10.1175/ MWR-D-18-0028.1.
41. Blake E. and M. Brennan, 2021. 2021 hurricane season summary. Tropical Cyclone Operations and Research Forum, Lakeland, FL.
42. Hortal, M., 2004. Overview of the numerics of the ECMWF atmospheric forecast model. *Recent developments in numerical methods for atmospheric and ocean modelling*. ECMWF.
43. ECMWF, 2020. IFS documentation. https://www.ecmwf.int/en/publications/ifs-documentation.
44. Hólm E., S. Lang, P. Lean, 2020. Continuous long-window data assimilation. ECMWF Newsletter, Number 163.
45. Bonavita, M., Isaksen L., & Hólm E. 2012. On the use of EDA background error variances in the ECMWF 4D-Var. *Quarterly Journal of the Royal Meteorological Society*, **138**, 1540–1559, doi:10.1002/qj.1899.
46. Mogensen, K.S., L. Magnusson, J.R. Bidlot, 2017: Tropical Cyclone Sensitivity to Ocean Coupling. Technical Memorandum 794, ECMWF. Available at https://www.ecmwf.int/en/publications/technical-memoranda.
47. Bonavita, M., M. Dahoui, P. Lopez, et al. 2017. On the initialization of tropical cyclones. ECMWF Tech. Memo. 810, http://www.aoml.noaa.gov/hrd/tcfaq/tcfaqHED.html.
48. Magnusson, L., Bidlot, J. R., Bonavita, M., *et al*. 2019. ECMWF activities for improved hurricane forecasts. *Bulletin of the American Meteorological Society*, 100(3), 445–457. https://doi.org/10.1175/BAMS-D-18-0044.1.
49. De Chiara, G., Bonavita, M., & English, S. J. 2017. Improving the Assimilation of Scatterometer Wind Observations in Global NWP. IEEE Journal of Selected Topics in Applied Earth Observations and *Remote Sensing*, 10(5), 2415–2423. https://doi.org/10.1109/JSTARS.2017.2691011.

50. Geer, A. J., K. Lonitz, P. Weston, *et al*. 2018. All-sky satellite data assimilation at operational weather forecasting centres. *Quarterly Journal of the Royal Meteorological Society*, **144**, 1191–1217, doi:10.1002/qj.3202.
51. Walters, D., Boutle, I., Brooks, M., et al. 2017. The Met Office Unified Model Global Atmosphere 6.0/6.1 and JULES Global Land 6.0/6.1 configurations. *Geoscientific Model Development*, *10*(4), 1487–1520. https://doi.org/10.5194/gmd-10-1487-2017
52. Heming, J. T., 2016. Met office unified model tropical cyclone performance following major changes to the initialization scheme and a model upgrade. *Weather and Forecasting*, **31**, 1433–1449, doi:10.1175/WAF-D-16-0040.1.
53. Putman, W. M., & Lin, S. J. 2007. Finite-volume transport on various cubed-sphere grids. *Journal of Computational Physics*, *227*(1), 55–78. https://doi.org/10.1016/j.jcp.2007.07.022
54. Zhou, L., Lin, S. J., Chen, J. H., Harris, et al. 2019. Toward convective-scale prediction within the next generation global prediction system. *Bulletin of the American Meteorological Society*, *100*(7), 1225–1243. https://doi.org/10.1175/BAMS-D-17-0246.1
55. Hong, S. Y., Noh, Y., & Dudhia, J. 2006. A new vertical diffusion package with an explicit treatment of entrainment processes. *Monthly Weather Review*, *134*(9), 2318–2341. https://doi.org/10.1175/MWR3199.1
56. Polland, R. T., Rhines, P. B., & Thompson, R. O. R. Y. 1973. The deepening of the wind-mixed layer. *Geophysical Fluid Dynamics*, 3, 381–404.
57. Chen, J. H., Lin, S. J., Magnusson, L., *et al.* 2019. Advancements in Hurricane Prediction With NOAA's Next-Generation Forecast System. *Geophysical Research Letters*, *46*(8), 4495–4501. https://doi.org/10.1029/2019GL082410
58. Kleist, D. T., & Ide, K. 2015. An OSSE-based evaluation of hybrid variational-ensemble data assimilation for the NCEP GFS. Part II: 4DEnVar and hybrid variants. *Monthly Weather Review*, *143*(2), 452–470. https://doi.org/10.1175/MWR-D-13-00350.1
59. Klest D., Treadon R., Thomas C., *et al.* 2021. NCEP Operational Global Data Assimilation Upgrades: From Versions 15 through 16. Special Symposium on Global and Mesoscale Models: Updates and Center Overviews and WAF Symposium. AMS Annual meeting, Virtual.
60. Hogan, T. F., Liu, M., Ridout, J. A., and et al. 2014. The navy global environmental model. *Oceanography*, *27*(3), 116–125. https://doi.org/10.5670/oceanog.2014.73
61. Xu, L., T. Rosmond, and R. Daley, 2005. Development of NAVDAS-AR: formulation and initial tests of the linear problem. *Tellus*, **57**, 546–559, doi:10.3402/tellusa.v57i4.14710.
62. Rosmond, T., and L. Xu, 2006: Development of NAVDAS-AR: Non-linear formulation and outer loop tests. *Tellus*, **58**, 45–58, doi:10.1111/j.1600-0870.2006.00148.x.
63. Kuhl D., T. Rosmond, C. Bishop, J. McLay, N.L. Baker, 2013. Comparison of hybrid ensemble/4DVar and 4DVar within the NAVDAS-AR data assimilation framework *Monthly Weather Review*, **141**, 2740-2758, doi:10.1175/MWR-D-12-00182.1
64. McLay, J. G., Bishop, C. H., & Reynolds, C. A., 2008: Evaluation of the ensemble transform analysis perturbation scheme at NRL. *Monthly Weather Review*, **136**, 1093–1108, doi:10.1175/2007MWR2010.1.
65. McLay, J., Bishop, C. H., & Reynolds, C. A., 2010: A local formulation of the ensemble transform (ET) analysis perturbation scheme. *Weather and Forecasting*, **25**, 985–993, doi:10.1175/2010WAF2222359.1.
66. Bishop, C. H., and Z. Toth, 1999. Ensemble transformation and adaptive observations. Journal of Atmospheric Sciences, 56, 1748-1765.

67. Goerss, J. S., and R. A. Jeffries, 1994. Assimilation of synthetic tropical cyclone observations into the Navy Operational Global Atmospheric Prediction System. *Weather and Forecasting*, **9**, 557- 576.
68. Reinecke A. and Coauthors, 2022: The Navy's Next-Generation NEPTUNE Modeling System. *31st Conference on Weather Analysis and Forecasting (WAF)/27th Conference on Numerical Weather Prediction (NWP)*, 2022 American Meteorology Society annual meeting, Houston, TX (virtual).
69. Giraldo, F.X. J.F. Kelly and E.M. Constantinescu, 2013. Implicit-Explicit Formulations for a 3D Nonhydrostatic Unified Model of the Atmosphere (NUMA), *SIAM Journal on Scientific Computing*. Vol. 35, Iss. 510.1137/120903038
70. Baker N., 2020. NRL science highlights and perspectives on the JCSDA. JCSDA quarterly newsletter No 68. https://doi.org/10.25923/kegw-5k19.
71. Kadowaki, T., Ota Y., and Yokota S. 2020. Introduction of a new hybrid data assimilation system for the JMA Global Spectral Model. *Research activities in Earth system modelling. Working Group on Numerical Experimentation. 1-09. WMO, Geneva.*
72. Yokota S., Kadowaki T., Oda M., Ota Y. 2021. Improving ensemble-based background error covariances of the hybrid 4DVar in JMA's global analysis. *Research activities in Earth system modelling. Working Group on Numerical Experimentation. 1-09. WMO, Geneva.*
73. Okamoto, K., McNally A. P., & Bell W. 2014. Progress towards the assimilation of all-sky infrared radiances: An evaluation of cloud effects. *Quarterly Journal of the Royal Meteorological Society*, 140, 1603–1614, https://doi.org/10.1002/qj.2242.
74. Shimizu H., Kazumori M., Kadowaki T. 2020. Implementation of all-sky microwave radiance assimilation into JMA's global NWP system. *Research activities in Earth system modelling. Working Group on Numerical Experimentation. 1-21. WMO, Geneva.*
75. JMA. (2019). Outline of the operational numerical weather prediction of the Japan Meteorological Agency. Japan Meteorological Agency. 180pp.
76. Ujiie, M., Higuchi M., Kadowaki T. *et al*. 2021. Upgrade of JMA's Operational Global NWP system. *Research activities in Earth system modelling. Working Group on Numerical Experimentation*, 6–07.
77. JMA 2018: JMA's NWP Strategic Plan Toward 2030: NWP innovation to ensure the safety and security of the people, and to realize a vibrant society. Available at: https://www.jma.go.jp/jma/en/Publications/JMA_NWP_Strategic_Plan_Toward_2030.pdf.
78. Doyle, J. D., Hodur, R. M., Chen, S., *et al.* 2014. Tropical cyclone prediction using COAMPS-TC. *Oceanography*, *27*(3), 104–115. https://doi.org/10.5670/oceanog.2014.72
79. Hsiao, L. F., D. S. Chen, Y. H. Kuo, *et al.* 2012. Application of WRF 3DVAR to operational typhoon prediction in Taiwan: Impact of outer loop and partial cycling approaches. *Weather and Forecasting*, **27**, 1249–1263, doi:10.1175/WAF-D-11-00131.1.
80. Hsiao, L. F., D. S. Chen, J. S. Hong, T. C. Yeh, and C. T. Fong, 2020. Improvement of the numerical tropical cyclone prediction system at the Central Weather Bureau of Taiwan: TWRF (Typhoon WRF). *Atmosphere*, **11**, doi:10.3390/atmos11060657.
81. Zhang, Z., M. Tong, J. Sippel, et al. 2020. The Impact of Stochastic Physics-Based Hybrid GSI/EnKF Data Assimilation on Hurricane Forecasts Using EMC Operational Hurricane Modeling System. *Atmosphere*, 11, 801, doi:10.3390/atmos11080801.
82. Tong, M., J. Sippel, V. Tallapragada, *et al.* 2018. Impact of assimilating aircraft reconnaissance observations on tropical cyclone initialization and prediction using operational HWRF and GSI ensemble-variational hybrid data assimilation. *Monthly Weather Review*, **146**, 4155–4177, doi:10.1175/MWR-D-17-0380.1.

83. Lu, X., Wang, X., Tong, M., & Tallapragada, V., 2017. GSI-Based, Continuously Cycled, Dual-Resolution Hybrid Ensemble–Variational Data Assimilation System for HWRF: System Description and Experiments with Edouard (2014). *Monthly Weather Review*, **145**, 4877-4898. doi:10.1175/MWR-D-17-0068.1.
84. Pu, Z., S. Zhang, M. Tong and V. Tallapragada. 2016: Influence of the self-consistent regional ensemble background error covariance on hurricane inner-core data assimilation with the GSI-based hybrid system for HWRF, *Journal of the Atmospheric Sciences*, 73, 4911-4925.
85. Aberson, S. D., K. J. Sellwood, and P. A. Leighton, 2017. Calculating dropwindsonde location and time from TEMP-DROP messages for accurate assimilation and analysis. *Journal of Atmospheric and Oceanic Technology*, **34**, 1673–1678, doi:10.1175/JTECH-D-17-0023.1.
86. Christophersen, H., A. Aksoy, J. Dunion, and K. J. Sellwood, 2017. The impact of NASA Global Hawk unmanned aircraft dropwindsonde observations on tropical cyclone track, intensity, and structure: Case studies. *Monthly Weather Review*, 145, 1817–1830.
87. Christophersen, H., Aksoy, A., Dunion, J. P., *et al*. 2018. Composite Impact of Global Hawk Unmanned Aircraft Dropwindsondes on Tropical Cyclone Analyses and Forecasts. *Monthly Weather Review*, *146*, 2297–2314. https://doi.org/10.1175/MWR-D-17-0304.1
88. Cione, J. J., G. Bryan, R. Dobosy, *et al*. 2020. Eye of the Storm: Observing Hurricanes with a Small Unmanned Aircraft System. *Bulletin of the American Meteorological Society*, **101**, E186–E205, doi:10.1175/BAMS-D-19-0169.1.
89. Cione, J. J., E. A. Kalina, E. W. Uhlhorn, A. M. Farber, and B. Damiano, 2016. Coyote unmanned aircraft system observations in Hurricane Edouard. *Earth and Space Sciences*, 370–380.
90. Wick. G., J. Dunion, P. Black, *et al*. 2020. NOAA's Sensing Hazards with Operational Unmanned Technology (SHOUT) Experiment Observations and Forecast Impact. *Bulletin of the American Meteorological Society*, **101**, E968–E987, doi:10.1175/BAMS-D-18-0257.1.
91. Braun, S. A., Kakar, R., Zipser, E., Heymsfield, et al. 2013. NASA's genesis and rapid intensification processes (GRIP) field experiment. *Bulletin of the American Meteorological Society*, *94*(3), 345–363. https://doi.org/10.1175/BAMS-D-11-00232.1
92. Braun, S. A., Newman, P. A., & Heymsfield, G. M. 2016. NASA's Hurricane and Severe Storm Sentinel (HS3) Investigation. *Bulletin of the American Meteorological Society*, *1990*(November), 2085–2102. https://doi.org/10.1175/BAMS-D-15-00186.1
93. Weissmann, M., F. Harnisch, C. Wu, *et al.* 2011. The influence of assimilating dropsonde data on Typhoon track and midlatitude forecasts. *Monthly Weather Review*, **139**, 908–920, doi:10.1175/2010MWR3377.1.
94. Wu, C. C., P. Lin, S. Aberson, *et al.* 2005. Dropwindsonde observations for typhoon surveillance near the Taiwan region (DOTSTAR): An overview. *Bulletin of the American Meteorological Society*, **86**, 787–790, doi:10.1175/BAMS-86-6-787.
95. Ditchek, S. D., J. Sippel, G. Alaka, *et al*. 2021. Quantifying the Overall and Radial Impacts of Dropsondes during the 2017–19 Hurricane Seasons Using the Basin-Scale HWRF. 101st Annual Meeting of the American Meteorological Society. 10-15 Jan., 2021.
96. Weng, Y. and F. Zhang, 2016. Advances in Convection-Permitting Tropical Cyclone Analysis and Prediction through EnKF Assimilation of Reconnaissance Aircraft Observations. *Journal of the Meteorological Society of Japan*, **94**, 345-358, doi:10.2151/jmsj.2016-018.
97. Aberson, S. D., A. Aksoy, K. J. Selwood, *et al.* 2015. Assimilation of High-Resolution Tropical Cyclone Observations with an Ensemble Kalman Filter Using HEDAS: Evaluation of 2008–11 HWRF Forecasts. *Monthly Weather Review,* **143**, 511-523.

98. Aksoy, A., S. Lorsolo, T. Vukicevic, *et al*. 2012. The HWRF Hurricane Ensemble Data Assimilation System (HEDAS) for High-Resolution Data: The Impact of Airborne Doppler Radar Observations in an OSSE. *Monthly Weather Review*, **141**, 1843–1862, doi:10.1175/MWR-D-11-00212.1.
99. Aksoy, A., S. D. Aberson, T. Vukicevic, *et al.* 2013. Assimilation of High-Resolution Tropical Cyclone Observations with an Ensemble Kalman Filter Using NOAA/AOML/HRD's HEDAS: Evaluation of the 2008–11 Vortex-Scale Analyses. *Monthly Weather Review*, **141**, 1842–1865, doi:10.1175/MWR-D-12-00194.1.
100. Zawislak, J., Rogers, R. F., Aberson, S. D., *et al*. 2021. Accomplishments of NOAA's Airborne Hurricane Field Program and a Broader Future Approach to Forecast Improvement. *Bulletin of the American Meteorological Society*, *103*(2), E311–E338. https://doi.org/10.1175/bams-d-20-0174.1
101. Zhang, F., Y. Weng, J. A. Sippel, et al. 2009. Cloud-Resolving Hurricane Initialization and Prediction through Assimilation of Doppler Radar Observations with an Ensemble Kalman Filter. *Monthly Weather Review*, **137**, 2105-2125.
102. Li, Y., X. Wang, and M. Xue, 2012. Assimilation of radar radial velocity data with the WRF hybrid ensemble-3dvar system for the prediction of Hurricane Ike (2008). *Monthly Weather Review*, **140**, 3507–3524, doi:10.1175/MWR-D-12-00043.1.
103. Dong, J., and M. Xue, 2013. Assimilation of radial velocity and reflectivity data from coastal WSR-88D radars using ensemble Kalman filter for the analysis and forecast of landfalling Hurricane Ike (2008). *Quarterly Journal of the Royal Meteorological Society*, **139**, 467–487, doi:10.1002/qj.1970.
104. Zhu, L., Q. Wan, X. Shen, *et al.* 2016. Prediction and Predictability of High-Impact Western Pacific Landfalling Tropical Cyclone Vicente (2012) through Convection-Permitting Ensemble Assimilation of Doppler Radar Velocity, *Monthly Weather Review*, **144**, 21-43, doi:10.1175/MWR-D-14-00403.1.
105. Yue, J., Meng, Z., 2017. Impact of assimilating Taiwan's coastal radar radial velocity on forecasting Typhoon Morakot (2009) in southeastern China using a WRF-based EnKF. *Science China Earth Sciences*, **60**, 315–327, doi:10.1007/s11430-015-0259-y.
106. Feng, J., Duan, Y., Wan, Q., *et al*. 2020. Improved Prediction of Landfalling Tropical Cyclone in China Based on Assimilation of Radar Radial Winds with New Super-Observation Processing, Weather and Forecasting, 35, 2523-2539. doi:10.1175/WAF-D-20-0002.1.
107. Wang, Y. and Pu Z. 2021. Assimilation of Radial Velocity from Coastal NEXRAD into HWRF for Improved Forecasts of Landfalling Hurricanes. *Weather and Forecasting*. 36, 587-599
108. Gao, J., and Stensrud, D. J., 2012. Assimilation of reflectivity data in a convective-scale, cycled 3DVAR framework with hydrometeor classification. *Journal of the Atmospheric Sciences*, **69**, 1054–1065.
109. Zhao, Q., and Jin, Y. 2008. High-resolution radar data assimilation for Hurricane Isabel (2003) at landfall. *Bulletin of the American Meteorological Society*, **09**, 1355–1372.
110. Wang, Y., and X. Wang, 2017. Direct assimilation of radar reflectivity without tangent linear and adjoint of the nonlinear observation operator in the GSI-based EnVar system: Methodology and experiment with the 8 may 2003 Oklahoma City tornadic supercell. *Monthly Weather Review*, **145**, 1447–1471, doi:10.1175/MWR-D-16-0231.1.

111. Aksoy, A., Dowell, D. C., and Snyder, C., 2009. A multicase comparative assessment of the ensemble Kalman filter for assimilation of radar observations. Part II: Short-range ensemble forecasts. *Monthly Weather Review*, **138**, 1273–1292. https://doi.org/10.1175/2009MWR3086.1
112. Weygandt, S., and Benjamin, S., 2007. Radar Reflectivity-based Initialization of Precipitation Systems using a Diabatic Digital Filter within the Rapid Update Cycle. Preprints, *18th Conf. Num. Wea. Pred*., June, 2–12.
113. Bresky, W. C., Daniels, J. M., Bailey, A. A., & Wanzong, S. T. 2012. New methods toward minimizing the slow speed bias associated with atmospheric motion vectors. *Journal of Applied Meteorology and Climatology*, *51*(12), 2137–2151. https://doi.org/10.1175/JAMC-D-11-0234.1
114. Nieman, S. J., W. P. Menzel, C. M. Hayden, *et al*. 1997. Fully automated cloud-drift winds in NESDIS operations. *Bulletin of the American Meteorological Society*, **78**, 1121–1133, https://doi.org/10.1175/1520-0477(1997)078<1121:FACDWI>2.0.CO;2.
115. Velden, C. S., J. Daniels, D. Stettner, *et al*. 2005. Recent innovations in deriving tropospheric winds from meteorological satellites. *Bulletin of the American Meteorological Society*, **86**, 205–223, https://doi.org/10.1175/BAMS-86-2-205.
116. Lim, A. H. N., J. A. Jung, S. E. Nebuda, *et al*. 2019. Tropical Cyclone Forecasts Impact Assessment from the Assimilation of Hourly Visible, Shortwave, and Clear-Air Water Vapor Atmospheric Motion Vectors in HWRF, *Weather and Forecasting*, **34**, 177-198, doi:10.1175/WAF-D-18-0072.1.
117. Zhang, S., Pu Z., & Velden C. 2018. Impact of enhanced atmospheric motion vectors on HWRF hurricane analysis and forecasts with different data assimilation configurations. *Monthly Weather Review*, 146, 1549-1569.
118. Velden, C., W. E. Lewis, W. Bresky, *et al*. 2017. Assimilation of High-Resolution Satellite-Derived Atmospheric Motion Vectors: Impact on HWRF Forecasts of Tropical Cyclone Track and Intensity, *Monthly Weather Review*, **145**, 1107-1125, doi:10.1175/MWR-D-16-0229.1.
119. Li, J., J. Li, C. Velden, P. Wang, et al. 2020. Impact of rapid-scan-based dynamical information from GOES-16 on HWRF hurricane forecasts. *Journal of Geophysical Research: Atmospheres*, **125**, e2019JD031647, doi:10.1029/2019JD031647.
120. Geer, A. J., Bauer, P., & Lopez, P. 2010. Direct 4D-Var assimilation of all-sky radiances. Part II: Assessment. *Quarterly Journal of the Royal Meteorological Society*, *136*(652), 1886–1905. https://doi.org/10.1002/qj.681
121. Duncan D. I., N., N. Bormann, A. J. Geer, *et al*. 2022. Assimilation of AMSU-A in all-sky conditions. *Monthly Weather Review,* https://doi.org/10.1175/MWR-D-21-0273.1.
122. Geer, A.J., Baordo, F., Bormann, N., *et al*. 2017. The growing impact of satellite observations sensitive to humidity, cloud and precipitation. *Quarterly Journal of the Royal Meteorological Society,* **143**, 3189-3206. doi:10.1002/qj.3172.
123. Zhu, Y., E. Liu, R. Mahajan, *et al*. 2016. All-sky microwave radiance assimilation in NCEP's GSI analysis system. *Monthly Weather Review*, **144**, 4709–4735, https://doi.org/10.1175/MWR-D-15-0445.1.
124. Zhu, Y., Gayno, G., Purser, R. J., *et al*. 2019. Expansion of the all-sky radiance assimilation to ATMS at NCEP. *Monthly Weather Review*, *147*(7), 2603–2620. https://doi.org/10.1175/MWR-D-18-0228.1
125. Tong, M., Zhu, Y., Zhou, L., *et al*. 2020. Multiple hydrometeors all-sky microwave radiance assimilation in FV3GFS. *Monthly Weather Review*, *148*(7), 2971–2995. https://doi.org/10.1175/MWR-D-19-0231.1
126. Migliorini, S., & Candy, B. 2019. All-sky satellite data assimilation of microwave temperature sounding channels at the Met Office. *Quarterly Journal of the Royal Meteorological Society*, *145*(719), 867–883. https://doi.org/10.1002/qj.3470

127. Kazumori, M., & Kadowaki, T. 2017. Development of an all-sky assimilation of microwave imager and sounder radiances for the Japan Meteorological Agency global numerical weather prediction system. *21st Int. TOVS Study Conf*., Darmstadt, Germany, International ATOVS Working Group, 9 pp., https://cimss.ssec.wisc.edu/itwg/itsc/itsc21/proceedings/5.04_kazumori.pdf.
128. Shahabadi, M. B., & Buehner, M. 2021. Toward all-sky assimilation of Microwave temperature sounding channels in environment Canada's global deterministic weather prediction system. *Monthly Weather Review*, *149*(11), 3725–3738. https://doi.org/10.1175/MWR-D-21-0044.1
129. Yang, C., Z. Liu, J. Bresch, S. R. H. Rizvi, X. Y. Huang, and J. Min, 2016. AMSR2 all-sky radiance assimilation and its impact on the analysis and forecast of Hurricane Sandy with a limited- area data assimilation system. Tellus, 68A, 30917, https://doi.org/10.3402/tellusa.v68.30917.
130. Xian, Z., K. Chen, and J. Zhu, 2019. All-sky assimilation of the MWHS-2 observations and evaluation the impacts on the ana- lyses and forecasts of binary typhoons. *Journal of Geophysical Research*, 124, 6359–6378, https://doi.org/10.1029/2018JD029658.
131. Wu, T. C., M. Zupanski, L. D. Grasso, C. D. Kummerow, and S. A. Boukabara, 2019: All-sky radiance assimilation of ATMS in HWRF: A demonstration study. *Monthly Weather Review*, 147, 85–106, https://doi.org/10.1175/MWR-D-17-0337.1.
132. Christophersen, H. W., Dahl, B. A., Dunion, J. P., Rogers, R. F., Marks, F. D., Atlas, R., & Blackwell, W. J. 2021. Impact of TROPICS Radiances on Tropical Cyclone Prediction in an OSSE. *Monthly Weather Review*, *149*, 2279–2298. https://doi.org/10.1175/mwr-d-20-0339.1
133. Chevallier, F., & Lopez, P. 2004. The capability of 4D-Var systems to assimilate cloud-affected satellite infrared radiances. *Quarterly Journal of the Royal Meteorological Society, 130*, 917–932.
134. Okamoto, K. 2017. Evaluation of IR radiance simulation for all-sky assimilation of Himawari-8/AHI in a mesoscale NWP system. *Quarterly Journal of the Royal Meteorological Society*, *143*(704), 1517–1527. https://doi.org/10.1002/qj.3022
135. Zhao, Q., Baker, N. L., Jin, Y., & Nystrom, R. (2021). Scale analysis of infrared water vapor brightness temperatures for tropical cyclone all-sky radiance assimilation. *Geophysical Research Letters*, *48,* e2021GL095458. https://doi.org/10.1029/2021GL095458
136. Honda, T., Miyoshi, T., Lien, G. Y., *et al*. 2018. Assimilating all-sky Himawari-8 satellite infrared radiances: A case of Typhoon Soudelor (2015). *Monthly Weather Review*, *146*(1), 213–229. https://doi.org/10.1175/MWR-D-16-0357.1
137. Minamide, M., and F. Zhang, 2018. Assimilation of all-sky Infrared radiances from Himawari-8 and impacts of moisture and hydrometer initialization on convection-permitting tropical cyclone prediction, *Monthly Weather Review*, 146, 3241-3258, doi:10.1175/MWR-D-17-0367.1.
138. Minamide, M, and F. Zhang, 2019. An adaptive background error inflation method for assimilating all-sky radiances. *Quarterly Journal of the Royal Meteorological Society*, **145**, 805–823, doi:10.1002/qj.3466.
139. Zhang, F., Minamide, M., Nystrom, R. G., *et al*. 2019. Improving harvey forecasts with next-generation weather satellites: Advanced hurricane analysis and prediction with assimilation of goes-r all-sky radiances. *Bulletin of the American Meteorological Society*, *100*(7), 1217–1222. https://doi.org/10.1175/BAMS-D-18-0149.1
140. Geer, A. J., & Bauer, P. 2011. Observation errors in all-sky data assimilation. *Quarterly Journal of the Royal Meteorological Society*, *137*(661), 2024–2037. https://doi.org/10.1002/qj.830
141. Okamoto, K., McNally, A. P., & Bell, W. 2014. Progress towards the assimilation of all-sky infrared radiances: An evaluation of cloud effects. *Quarterly Journal of the Royal Meteorological Society*, *140*(682), 1603–1614. https://doi.org/10.1002/qj.2242

142. Chambon, P., Zhang, S. Q., Hou, A. Y., *et al*. 2014. Assessing the impact of pre-GPM microwave precipitation observations in the Goddard WRF ensemble data assimilation system. *Quarterly Journal of the Royal Meteorological Society*, *140*(681), 1219–1235. https://doi.org/10.1002/qj.2215
143. Minamide, M., & Zhang, F. 2017. Adaptive observation error inflation for assimilating all-Sky satellite radiance. *Monthly Weather Review*, *145*(3), 1063–1081. https://doi.org/10.1175/MWR-D-16-0257.1
144. Bishop, C. H., 2019. Data assimilation strategies for state-dependent observation error variances. *Quarterly Journal of the Royal Meteorological Meteorological Society*, 217–227, https://doi:10.1002/qj.3424.
145. Bonavita, M., L. Isaksen, and E. Hólm, 2012. On the use of EDA background error variances in the ECMWF 4D-Var. *Quarterly Journal of the Royal Meteorological Society*, **138**, 1540–1559, doi:10.1002/qj.1899.
146. Chen, Y., & Snyder, C. 2007. Assimilating Vortex Position with an Ensemble Kalman Filter. *Monthly Weather Review*, *135*(5), 1828–1845. https://doi.org/10.1175/MWR3351.1
147. Hamill, T. M., Whitaker, J. S., & Snyder, C. 2001. Distance-dependent filtering of background error covariance estimates in an ensemble Kalman filter. *Monthly Weather Review*, *129*(11), 2776–2790. https://doi.org/10.1175/1520-0493(2001)129<2776:DDFOBE>2.0.CO;2
148. Poterjoy, J., F. Zhang, and Y. Weng, 2014. The Effects of Sampling Errors on the EnKF Assimilation of Inner-Core Hurricane Observations. *Monthly Weather Review*, **142**, 1609–1630, doi:10.1175/MWR-D-13-00305.1.
149. Ménétrier, B., Montmerle, T., Michel, Y., *et al*. 2015. Linear filtering of sample covariances for ensemble-based data assimilation. Part I: Optimality criteria and application to variance filtering and covariance localization. *Monthly Weather Review*, *143*(5), 1622–1643. https://doi.org/10.1175/MWR-D-14-00157.1
150. Ikuta Y. 2016. Impact of flow-dependent assimilation using adjoint model including three-ice microphysics scheme. In: 4th International Workshop on Non-hydrostatic Models, 30 November–2 December, 2016, Hakone, Japan.
151. Zhang R., W. Zhang, Y. Zhang, *et al*. 2020. Application of Lightning Data Assimilation to Numerical Forecast of Super Typhoon Haiyan (2013). *Journal of Meteorological Research*, **34**,1052–1067.
152. Zupanski M., Zhang M., K. Apodaca, L. Grasso, J. Knaff, 2012. Utility of GOES-R instruments for hurricane data assimilation, The 10th JCSDA Workshop on Satellite Data Assimilation, College Park, MD.
153. Zhang, J. A., Atlas R., Emmitt G. D., *et al*. 2018. Airborne doppler wind lidar observations of the tropical cyclone boundary layer. *Remote Sensing*, **10**, 1–15, https://doi.org/10.3390/rs10060825.
154. Bucci L. R. 2020. Assessment of the Utility of Doppler Wind Lidars for Tropical Cyclone Analysis and Forecasting. University of Miami PhD dissertation. Retrieved from https://scholarship.miami.edu/discovery/fulldisplay?docid=alma991031496889502976&context=L&vid=01UOML_INST:ResearchRepository&lang=en&search_scope=ResearchETD&adaptor=Local%20Search%20Engine&tab=Research&query=any,contains,bucci&offset=0.
155. Pu, Z., L. Zhang, and G. D. Emmitt, 2010. Impact of airborne Doppler Wind Lidar data on numerical simulation of a tropical cyclone, *Geophysical Research Letters*, 37, L05801, doi:10.1029/2009GL041765.

156. Aksoy, A., Cione, J. J., Dahl, B. A., *et al*. 2022. Tropical Cyclone Data Assimilation with Coyote Uncrewed Aircraft System Observations, Very Frequent Cycling, and a New Online Quality Control Technique, *Monthly Weather Review*, 150(4), 797-820, https://doi.org/10.1175/MWR-D-21-0124.1.
157. Kren, A. C., Cucurull, L., & Wang, H. 2018. Impact of UAS Global Hawk Dropsonde Data on Tropical and Extratropical Cyclone Forecasts in 2016, *Weather and Forecasting*, 33(5), 1121-1141, https://doi.org/10.1175/WAF-D-18-0029.1.
158. Buehner, M., and A. Shlyaeva, 2015. Scale-dependent background-error covariance localisation. *Tellus A: Dynamic Meteorology and Oceanography*, 6, doi:10.3402/tellusa.v67.28027.
159. Huang, B., X. Wang, D. T. Kleist, *et al.* 2020. A Simultaneous Multiscale Data Assimilation Using Scale-Dependent Localization in GSI-Based Hybrid 4DEnVar for NCEP FV3-Based GFS. *Monthly Weather Review*, **149**, 479–501, doi:10.1175/mwr-d-20-0166.1.
160. Wang, X., H. G. Chipilski, C. H. Bishop, *et al*. 2020. A Multiscale Local Gain Form Ensemble Transform Kalman Filter (MLGETKF). *Monthly Weather Review*, 605–622, doi:10.1175/mwr-d-20-0290.1.
161. van Leeuwen P. J., 2019. Machine Learning meets Data Assimilation, 1st workshop on Leveraging AI in the Exploitation of satellite Earth observations and numerical weather prediction, College Park, MD.
162. Hodyss, D., 2011. Ensemble state estimation for nonlinear systems using polynomial expansions in the innovation. *Monthly Weather Review*, **139**, 3571–3588, doi:10.1175/2011MWR3558.1.
163. Bishop, C.H., 2016. The GIGG-EnKF: Ensemble Kalman filtering for highly skewed non-negative uncertainty distributions. *Quarterly Journal of the Royal Meteorological Meteorological Society*, **142**, 1395-1412. doi:10.1002/qj.2742.
164. Geer A., 2019. Opportunities for using AI methods in weather forecasting at ECMWF, 1st workshop on Leveraging AI in the Exploitation of satellite Earth observations and numerical weather prediction, College Park, MD.
165. Steward, J. L., J. E. Roman, A. L. Daviña, and A. Aksoy, A., 2018. Parallel direct solution of the covariance-localized ensemble square root Kalman filter equations with matrix functions, *Monthly Weather Review*, **146**, 2819-2836, doi:10.1175/MWR-D-18-0022.1.
166. Steward J. L., A. Aksoy, and Z. S. Haddad, 2017. Parallel direct solution of the ensemble square root Kalman filter equations with observation principal components, *Journal of Atmospheric and Oceanic Technology*, **34**, 1867-1884, doi:10.1175/JTECH-D-16-0140.1.
167. Velden, C. S., T. Olander, and S. Wanzong, 1998: The Impact of Multispectral GOES-8 Wind Information on Atlantic Tropical Cyclone Track Forecasts in 1995. Part 1: Dataset Methodology, Description and Case Analysis. *Mon. Wea. Rev.*, 126, 1202-1218.
168. Goerss, J., C. Velden, and J. Hawkins, 1998: The Impact of Multispectral GOES-8 Wind Information on Atlantic Tropical Cyclone Track Forecasts in 1995. Part 2: NOGAPS Forecasts. *Mon. Wea. Rev.*, 126, 1219-1227.
169. Stettner, D., C. Velden, R. Rabin, S. Wanzong, J. Daniels, and W. Bresky, 2019: Development of enhanced vortex-scale atmospheric motion vectors for hurricane applications. *Remote Sensing*, Volume 11, Issue 17.
170. Lewis, W. E., C. Velden, and D. Stettner, 2020: Strategies for Assimilating High-Density Atmospheric Motion Vectors into a Regional Tropical Cyclone Forecast Model (HWRF). *Atmosphere*, *11*, 673-691. https://doi.org/10.3390/atmos11060673.